Progress in Surface Science xxx (2017) xxx–xxx

Contents lists available at ScienceDirect

Progress in Surface Science

journal homepage: www.elsevier.com/locate/progsurf

Review article

Two-dimensional silica opens new perspectives

Christin Büchner, Markus Heyde *

Fritz-Haber-Institut der Max-Planck-Gesellschaft, Faradayweg 4-6, 14195 Berlin, Germany

ARTICLE INFO

Article history:
Available online xxxx

Keywords:
Two-dimensional glass
Vitreous
Amorphous
Zachariasen
Random continuous network
Crystalline
2D insulator
2D materials
2D silica
2D silicon dioxide
Silica bilayer
SiO_2
Graphene
Transfer
Band gap
Dielectric
Exfoliation
Atomic force microscopy
Scanning tunneling microscopy
Transmission electron microscopy

ABSTRACT

In recent years, silica films have emerged as a novel class of two-dimensional (2D) materials. Several groups succeeded in epitaxial growth of ultrathin SiO_2 layers using different growth methods and various substrates. The structures consist of tetrahedral [SiO_4] building blocks in two mirror symmetrical planes, connected via oxygen bridges. This arrangement is called a silica bilayer as it is the thinnest 2D arrangement with the stoichiometry SiO_2 known today. With all bonds saturated within the nano-sheet, the interaction with the substrate is based on van der Waals forces. Complex ring networks are observed, including hexagonal honeycomb lattices, point defects and domain boundaries, as well as amorphous domains. The network structures are highly tuneable through variation of the substrate, deposition parameters, cooling procedure, introducing dopants or intercalating small species.

The amorphous networks and structural defects were resolved with atomic resolution microscopy and modeled with density functional theory and molecular dynamics. Such data contribute to our understanding of the formation and characteristic motifs of glassy systems. Growth studies and doping with other chemical elements reveal ways to tune ring sizes and defects as well as chemical reactivities. The pristine films have been utilized as molecular sieves and for confining molecules in nanocatalysis. Post growth hydroxylation can be used to tweak the reactivity as well.

The electronic properties of silica bilayers are favourable for using silica as insulators in 2D material stacks. Due to the fully saturated atomic structure, the bilayer interacts weakly with the substrate and can be described as quasi-freestanding. Recently, a mm-scale film transfer under structure retention has been demonstrated. The chemical and mechanical stability of silica bilayers is very promising for technological applications in 2D heterostacks.

Due to the impact of this bilayer system for glass science, catalysis and the field of 2D materials, a large number of theoretical and experimental studies on silica bilayers have been reported in the last years. This review aims to provide an overview on the insights gained on this material and to point out opportunities for further discovery in various fields.

Abbreviations: 2D, two-dimensional; 3D, three-dimensional; AES, Auger electron spectroscopy; AFM, atomic force microscopy; DFT, density functional theory; EELS, electron energy loss spectroscopy; ESEM, environmental scanning electron microscopy; Gr, graphene; IRAS, infrared reflection absorption spectroscopy; LEED, low energy electron diffraction; LEEM, low energy electron microscopy; MD, molecular dynamics; ML, monolayer; ND, neutron diffraction; NMR, nuclear magnetic resonance spectroscopy; NP, nanoparticle; PMMA, poly(methyl methacrylate); SBU, secondary building unit; SPM, scanning probe microscopy; STM, scanning tunneling microscopy; STEM, scanning transmission electron microscopy; STS, scanning tunneling spectroscopy; TEM, transmission electron microscopy; TBPB, 1,3,5-tris(4-bromophenyl) benzene; UHV, ultra-high vacuum; UV–vis, ultraviolet–visible spectroscopy; XPEEM, X-ray photoemission electron microscopy; XPS, X-ray photoelectron spectroscopy; XRD, X-ray diffraction.

* Corresponding author.
E-mail address: heyde@fhi-berlin.mpg.de (M. Heyde).

https://doi.org/10.1016/j.progsurf.2017.09.001
0079-6816/

Please cite this article in press as: C. Büchner, M. Heyde, Two-dimensional silica opens new perspectives, Prog. Surf. Sci (2017), https://doi.org/10.1016/j.progsurf.2017.09.001

Contents

1. Introduction

Silicon dioxide in its crystalline and glassy forms is of immense technological importance, with applications ranging from cladding skyscraper facades to manufacturing microchips. Knowledge and control of the structure are key for designing the right materials for each purpose. At the same time, silicates are abundant in nature, and understanding their structures is equally crucial for geology and plant science. Recently, a new class of ultrathin silica films was created, which allows unique insights and control over the atomic structure.

These films are typically grown 'bottom up', with building blocks deposited from the vapor phase, allowing finely tuned film thickness. Supported by metal substrates, their properties can be explored with various tools from surface science. This material class has garnered a great deal of attention over the last years, with publications reporting on structural, chemical and electronic properties employing a large number of techniques.

This review aims to summarize the current state of research on silica bilayer systems, and to point out gaps in the knowledge as well as future potential of this material class. A number of well-defined silica thin film structures have been presented at this point, all of them formed by tetrahedral [SiO_4] building blocks, as shown in Fig. 1a. Monolayers (ML) of these building blocks form highly ordered honeycomb lattices with the film stoichiometry $SiO_{2.5}$ [1], where three oxygen bridges are formed to neighboring tetrahedra, while the fourth oxygen bridge is connected to the substrate [2]. A side view schematic is shown in Fig. 1b. Since these films exhibit one covalent bond to the substrate per structural unit, their atomic structure is strongly directed by the substrate and it is not expected that monolayer silica films can exist without a support.

By adapting the preparation of silica thin films, it is possible to grow layers with two tetrahedral building units stacked on top of each other, connected by an oxygen bridge [3]. Since the remaining three oxygen bonds per structural unit are connected in-plane, this system exhibits no covalent bonds to the substrate, and also no dangling bonds, as shown in Fig. 1c. This film is frequently denoted as bilayer silica film or two-dimensional (2D) silica. In analogy to other 2D materials like graphene (Gr) and phosphorene, the 2D silica film has also been labelled as silicatene, although it does not possess any unsaturated

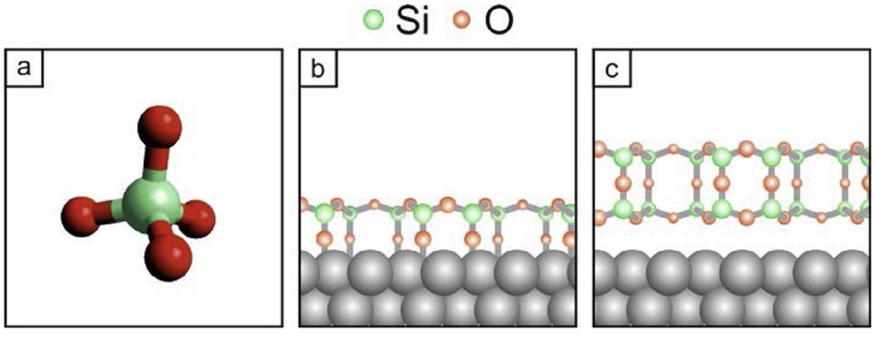

Fig. 1. Structure elements of silica layers. a) [SiO_4] tetrahedral building block. b) Side view of a monolayer film on a metal substrate. Tetrahedral building blocks are covalently bound to the substrate. c) Side view of bilayer film on a metal substrate. Tetrahedral building blocks of the top and the bottom layer are connected by perpendicular oxygen bridges in a mirror plane. The self-saturated oxide film interacts weakly with the substrate.

Please cite this article in press as: C. Büchner, M. Heyde, Two-dimensional silica opens new perspectives, Prog. Surf. Sci (2017), https://doi.org/10.1016/j.progsurf.2017.09.001

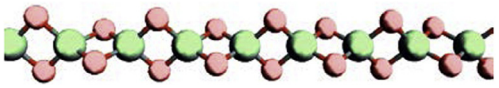

Fig. 2. Structure of W-silica, consisting of edge-connected [SiO_4] tetrahedra. Green spheres represent Si, red spheres represent O. Adapted from [6]. (For interpretation of the references to color in this figure legend, the reader is referred to the web version of this article.)

bonds (double bonds), which warrant the suffix –*ene* from the viewpoint of chemical nomenclature. When we use the term 2D SiO_2 or 2D silica throughout this text, we refer to the silica bilayer shown in Fig. 1c, which represents the thinnest possible sheet structure of the stoichiometry SiO_2.

As a consequence of the atomic structure, the epitaxial influence of the respective substrate is weaker than for the monolayer film, and 2D-amorphous silica bilayers have been observed [4]. We use the term amorphous to describe bilayer films that exhibit a variety of ring sizes, arranged in a 2D sheet without periodicity or long-range order. In the context of inorganic network glasses such as silica glass, this structural property is often called *vitreous*, while the term *amorphous* is applied to a wider range of materials, including amorphous polymers and metals [5].

When the [SiO_4] tetrahedra are connected via edges instead of corners, a chain-like arrangement of edge-sharing tetrahedra forms, which is coordinatively saturated, as shown in Fig. 2. Hence, this so-called W-silica can be seen as a one-dimensional analogy to silica bilayers. Such fibrous silica chains have been prepared by oxidizing SiO, but the resulting fibers were found to be unstable against moisture, which leads to the formation of silicic acid [6].

2D silica on the other hand is sufficiently mechanically and chemically stable to be isolated from the growth substrate. In this review, we focus on self-saturated bilayer sheets built from [SiO_4] tetrahedra and summarize the insights gained from these complex networks. For a comparative treatment of monolayer films, bilayer films and other ultra-thin silica structures, the reader is pointed to another recent review paper [7]. Alternative 2D silica structures that have been only computationally predicted at this point will not be a focus of this article [8–10].

Section 2 will describe the preparation procedures that have been reported for 2D silica films in the literature. Known factors influencing the growth will be highlighted and our current understanding of the film formation will be summarized.

Section 3 begins with an overview of the different characterization techniques that have been applied to the silica bilayer system, both experimentally and theoretically. As silica materials are ubiquitous in everyday life, the ability to obtain structural and chemical information on a silica system in unprecedented spatial resolution has implications for a number of research fields. We will consider the insights gained from silica bilayers on defect structures, on amorphous networks, on local structure–property relationships and on advanced microscopy techniques. In Section 4, we will discuss the studies that have been presented on chemical modification of silica bilayers through metal doping or through post-growth hydroxylation. We will also review the new possibilities that this thin film system provides for studying model catalysis.

Section 5 reviews the potential role of silica bilayers in material science and the state of knowledge regarding material properties of 2D silica.

2. Preparation of silica bilayers

In this section, we describe the reported preparations of silica bilayers, providing context by including the typical preparation of silica monolayers. Here, we only deal with pristine SiO_2 films, whereas Section 4 will deal with chemical functionalization and introduction of dopants into the network. As of writing this review, silica bilayers have been prepared on several metal single crystal substrates – Ru(0 0 0 1) [3,4], Pt(1 1 1) [11], Pd(1 0 0) [12], and Pd(1 1 1) [13], as well as on a Pd(1 1 1) thin film [13], a NiPd(1 1 1) alloy thin film [14], Ru- and Co-nanoparticles [15] (NP), and graphene-covered Cu-foils [16].

The preparation procedures for the metal single crystals and the metal thin films follow the common approach of physical vapor deposition with subsequent annealing. The preparation on Ru-NP, Co-NP and Gr/Cu can be described as solid state growth processes.

Molybdenum substrates were employed early on to grow ultrathin silica films, establishing many of the preparation principles still used today to obtain 2D SiO_2 layers [17–19]. The first reported preparation of a well-ordered ultrathin silica layer is the $SiO_{2.5}$ monolayer on Mo(1 1 2) [2,20]. The cleaned substrate was exposed to an oxygen atmosphere prior to deposition of a well-defined amount of silicon from an e-beam evaporator at room temperature in the oxygen environment. Both sequential [2] and one-step deposition [20] of the required Si amount have been described with similar results. A high-temperature (values reported between 800 and 1200 K) annealing step in O_2 or in ultra-high vacuum (UHV) facilitated the formation of a flat, highly ordered film [2,20]. Depositing larger amounts of Si on Mo substrates resulted in the formation of poorly-defined films, which, upon annealing, either showed decomposition or material loss leading to a monolayer [7]. This behavior indicates a self-limiting growth mechanism for monolayer films on Mo(1 1 2).

A structurally equivalent $SiO_{2.5}$ monolayer can be obtained with Ru(0 0 0 1) as substrate. However, the film growth on ruthenium exhibits no self-limitation at 1 ML. Changing the substrate from Mo(1 1 2) to Ru(0 0 0 1) allows the growth of silica bilayers with hexagonal or amorphous network morphologies with only minor adaptations to this preparation procedure. Cleaned Ru(0 0 0 1) surfaces were heated in O_2 to achieve a precoverage of either $(2 \times 1)O$ [3] or $(2 \times 2)3O$ [4]. The latter

Please cite this article in press as: C. Büchner, M. Heyde, Two-dimensional silica opens new perspectives, Prog. Surf. Sci (2017), https://doi.org/10.1016/j.progsurf.2017.09.001

coverage is achieved by only reducing the oxygen partial pressure after cooling the sample below 470 K. The Si deposition step can be carried out sequentially [21] or in a single step [3,4], achieving comparable outcomes. Si is dosed from an e-beam evaporator in an oxygen atmosphere, and sample temperatures for deposition from 100 K [21] to 630 K [3] have been reported. One study investigated silica nucleation density and island size as a function of sample temperature during deposition [22], showing that above 1000 K, silica building units have a lower sticking probability on the surface.

Annealing the sample in oxygen around 1200 K yields flat, fully oxidized films with the bilayer structure indicated in Fig. 1c. A low energy electron microscopy (LEEM) and X-ray photoelectron emission microscopy (XPEEM) study established an optimum temperature range for annealing silica bilayers between 1020 K and 1180 K [22], below which suboxide species are observed, and above which dewetting is observed. These high annealing temperatures are explained with a large activation energy which was found for the island formation [22]. Depositing Si exceeding the amount required for bilayer formation resulted in thicker, unordered films [21].

The preparation of SiO_2 on Pt(1 1 1) followed the same procedure as for Ru(0 0 0 1) substrates, performing the deposition step at a sample temperature of 100 K [11].

SiO_2 bilayers on Pd(1 0 0) and Pd(1 1 1) have been prepared without a O precover, depositing Si from a heated Si wafer at a sample temperature of 500–600 K [12,13]. The annealing step was carried out in oxygen between 1000 K and 1100 K. An alternative preparation deposited SiO_2 in excess of 2 ML, resulting in unordered films initially. During prolonged heating, however, the excess materials either evaporated or migrated into the bulk, so that a highly-ordered bilayer emerged [13,23]. This behavior shows similarities to the self-limiting growth of $SiO_{2.5}$ monolayer films.

Although the preparations on metal single crystals described above follow a similar pattern, different outcomes in terms of film morphology have been observed. Several studies have therefore identified the choice of substrate as a crucial parameter that governs the growth of the 2D silica film. The observed differences in film formation on Mo(1 1 2), Ru(0 0 0 1) and Pt (1 1 1) substrates led to conclusions about chemical affinities directing film growth [11]. While on Mo(1 1 2), self-limiting growth of ordered monolayer silica has been observed, Ru(0 0 0 1) allows monolayer and bilayer structures, depending on the deposited amount. In the case of ruthenium, coexistence of hexagonally ordered and amorphous bilayers has also been observed [24]. Furthermore, Pt(1 1 1) as a substrate yields only bilayer films with exclusively amorphous topologies. The additional observation that the metal oxygen affinity is highest for molybdenum and lowest for platinum, indicates that the strength of Me-O-Si (Me = substrate metal) bonds that are presumably formed during the film growth, directly influences the layered structures and the network topology [11].

Substrate influence also has been addressed in terms of symmetry and epitaxial strain caused by a lattice mismatch between substrate and film, and Table 1 shows reported lattice constants for several systems. Density functional theory (DFT) calculations predict free-standing silica bilayers to have a lattice constant of 5.3 Å [12,25,26]. This unit cell is stretched to 5.42 Å for crystalline silica bilayers on Ru(0 0 0 1) and 5.50 Å on Pd(1 0 0). The resulting strain lowers the energetic cost for the introduction of ring sizes other than the six-membered rings that comprise the crystalline phase [26]. Amorphous domains, or periodic domain boundaries, which will be discussed in detail in Section 3, can be viewed as such strain-relieving structural elements. In the case of a square substrate lattice like Pd(1 0 0), antiphase-domain boundaries are the result of relaxation of the 2D silica film in the incommensurate substrate direction [12].

When Pd(1 1 1) is used as a substrate, the lattice mismatch is too large to be compensated by a stretching of the silica film. Instead, incommensurate growth of a crystalline film is observed, resulting in a moiré pattern [13].

A recent study showed the preparation on an alloy thin film, which allows controlling the unit cell by varying the concentration of each component [14]. A 50 nm thick film with 48% Ni and 52% Pd was prepared on an oxide support, exposing a (1 1 1) facet. The resulting surface unit cell with a = 2.63 Å has a very small mismatch with the freestanding hexagonal SiO_2 bilayer (a = 5.3 Å [26]), which results in the growth of a well ordered, low defect honeycomb layer [14].

In addition to the substrate, the amount of SiO_2 on the surface also influences the atomic structure of the bilayer films. While SiO_2 monolayers form hexagonally ordered lattices on Ru(0 0 0 1), coverages of 1.4 ML and more yield the formation of bilayer structures while exposing parts of the substrate. From 1.4 ML to about 1.8 ML, the bilayer films exhibit predominantly amorphous bilayer structures, while at higher coverages predominantly crystalline bilayers are observed [27]. This effect has been linked to the reduced density of amorphous silica layers, allowing them to spread over a larger share of the substrate and thus minimizing the system's surface energy [26].

Two other preparation procedures of silica bilayers have been reported, which do not provide Si or SiO_2 as a component via the gas phase. Instead, the film growth substrate is situated on a thicker SiO_2 support, which allows small quantities of SiO_2 to migrate to the growth substrate, forming a bilayer. Hence, both preparation methods fall under the category of solid state growth.

Table 1
Reported lattice constants for 2D SiO_2 films on different substrates.

Support	Lattice constant (ordered films)	Technique, Reference
Freestanding	5.30 Å	DFT [12]
SiO_2/Ru(0 0 0 1)	5.42 Å	LEED, STM, AFM [3]
SiO_2/Pd(1 0 0)	5.50 Å	LEED [12]
SiO_2/Graphene	5.30 Å	TEM nanodiffraction [16]

Please cite this article in press as: C. Büchner, M. Heyde, Two-dimensional silica opens new perspectives, Prog. Surf. Sci (2017), https://doi.org/10.1016/j.progsurf.2017.09.001

A thin copper foil on a quartz substrate has been exposed to hexane vapor at 1223 K with the intention of growing graphene on copper [16]. Accidental air leakage into the chamber is assumed to have oxidized the Cu surface and caused the formation of a silica bilayer between graphene and copper by partial Si or SiO_2 migration from the support to the Gr/Cu interface. By subsequent etching of the Cu foil, a graphene/2D silica stack was obtained [16].

A study comparing the solid state growth of silica bilayers on Ru, Co and Fe provides some insight into the growth mechanism for this preparation route [15,28]. On 10 nm thick SiO_2 layers, 5 nm layers of the respective metal were sputter-deposited and annealed at 973 K, leading to the formation of metal nanoplatelets. Upon cooling samples to 723 K, the formation of thin silica layers was observed. For Ru and Co, these structures were assigned to silica bilayers, while for Fe, the formation of monolayers was concluded [15]. Following the film growth in-situ, preferential nucleation at the metal grain boundaries was observed, indicating that Si (and possibly O) from the support migrates through the metal nanoplatelets, forming thin silica films on the surface [28]. In these experiments, no additional oxygen was provided during the preparation. The oxygen incorporated in the silica films was concluded to stem either from the SiO_2 substrate or from an inherent oxide layer on the metal [15].

A common trait of the presented growth methods is the requirement of a highly clean substrate. Studies with metal single crystal substrates were conducted in UHV after cycles of sputtering and annealing the surface until the amount of impurities dropped below the detection level of either Auger electron spectroscopy (AES) or X-ray photoelectron spectroscopy (XPS). The solid-state growth studies highlight the need to clean the metal surface with an intense "beam shower" of electrons, only after which well-ordered films nucleated [15]. In accordance with these observations, one might assume that the copper foil used as substrate in [16] was covered by graphene, blocking adsorbates from above and facilitating the growth of a silica film from below.

Summarizing the reported preparation procedures, a number of experimental parameters emerge that influence the structure of the final silica bilayer. These parameters are

- Substrate choice
- Thermal treatment
- Coverage
- Dopant species

and are shown schematically in Fig. 3. Varying these factors allows structural and chemical tuning of the silica films.

The various reports on 2D silica preparations have commented on a number of other preparation parameters, implying further opportunities to influence the final structure of silica bilayers. However, a full understanding of these influencing factors will require more systematic investigations.

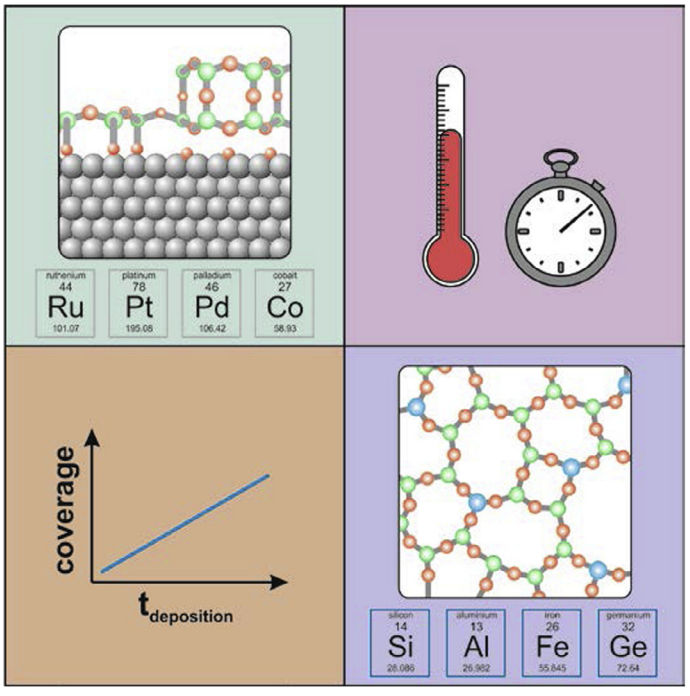

Fig. 3. Among the preparation parameters influencing silica film structures are substrate choice, thermal treatment, coverage, and dopants.

Please cite this article in press as: C. Büchner, M. Heyde, Two-dimensional silica opens new perspectives, Prog. Surf. Sci (2017), https://doi.org/10.1016/j.progsurf.2017.09.001

The transition of silica films between the liquid and solid state still holds some mysteries. Several reports point out that fast cooling is crucial to bypass the crystallization process and obtain an amorphous structure and hence the cooling rate is a crucial parameter [1,4]. While cooling rates of 1 K/s yielded films with coexisting crystalline and amorphous domains [22,29], a further systematic study of cooling rates might prove insightful. It has also been observed that a well-defined bilayer can be formed by depositing and annealing a monolayer each in two consecutive steps [7], but a fully formed bilayer cannot be grown into thicker films. Furthermore, holes in a fully oxidized bilayer could not be filled by depositing more Si and performing an additional oxidation step [22].

Some insights have been presented on the role of O partial pressure during the film formation. According to a phase diagram based on DFT calculations, a silica bilayer is the most stable structure for high Si coverages, over a wide range of oxygen partial pressures [21]. Different O activities during the film preparation can yield different O adsorbate coverages at the interface between metal and oxide film. Switching reversibly between an O-rich and an O-poor configuration without compromising the silica film has been demonstrated [30]. Another study points out that there should exist an ideal O pressure range, below which the SiO_2 film decomposes, and above which the substrate forms a bulk oxide [26].

Studies on vapor deposited molecular glasses and on metallic glasses indicate that deposition at lower rates and just below the glass transition temperature T_g provides the glass forming moieties with sufficient mobility to diffuse across the surface and form lower energy structures than those accessible by quenching a corresponding liquid [31,32]. It has also been observed that while the long-term changes in glass are negligible at ambient temperature [33], annealing temperatures several hundred degrees below the glass transition temperature for weeks or months can induce structural changes and crystallization of the material [34]. In view of the general relationship between enhanced surface mobility and lower energy glass structures, a systematic investigation of deposition rates vs. deposition temperatures or annealing times vs. annealing temperatures seems prudent, as using lower annealing temperatures in particular would allow a wider range of possible substrate materials.

Finally, potential alternative preparation approaches for silica bilayers need to be addressed. The main drawback in the current procedures used for film preparation is the lack of scalability, a detriment shared by all vacuum-based techniques. For industrial applications, the cost of materials, the size of films which can be grown and practical methods to manipulate films have to be considered. As has recently been shown, silica bilayers can be supported by metal thin films, which is more economical than metal single crystals [14]. By adapting deposition and heating setups to perform uniformly beyond the current cm-scale, larger films may successfully be grown. Chemical vapor deposition using appropriate precursor molecules may be an alternative route to prepare 2D silica films, analogous to the recent successes in preparing large-scale graphene sheets [35]. Exfoliating vapor-grown films can produce well-defined 2D silica sheets [36], but suffers from low throughput and is therefore only feasible in fundamental research. Especially for the group of aluminosilicates, other nanofabrication methods have been developed, which can inspire the production of 2D silica layers going forward.

Tectosilicate or zeolite layers with a mixture of $[SiO_4]$ and $[AlO_4]$ tetrahedra can be prepared bottom-up from a solution of molecular precursors. The layers can be either spin coated or self-assembled in solution with structure directing agents, and films as thin as 2 nm have been obtained [37,38]. Solution-based self-assembly is still an active field of research, and recently a novel template-free approach was presented to obtain silica nanosheets of 5–7 nm thickness through anisotropic interaction of nanoparticles [39].

Another common approach for the preparation of thin films is the top-down exfoliation of a layered solid. 1.3 nm thick zeolite nanosheets were exfoliated from layered MCM-22 [41]. Hexacelsians are a subgroup of the sheet-like silicates (phyllosilicates), which have been prepared from other silicate polymorphs via high temperature and high pressure routes, but remain stable at normal conditions [40,42,43]. As shown in Fig. 4, they consist of non-branched double layers of tetrahedra,

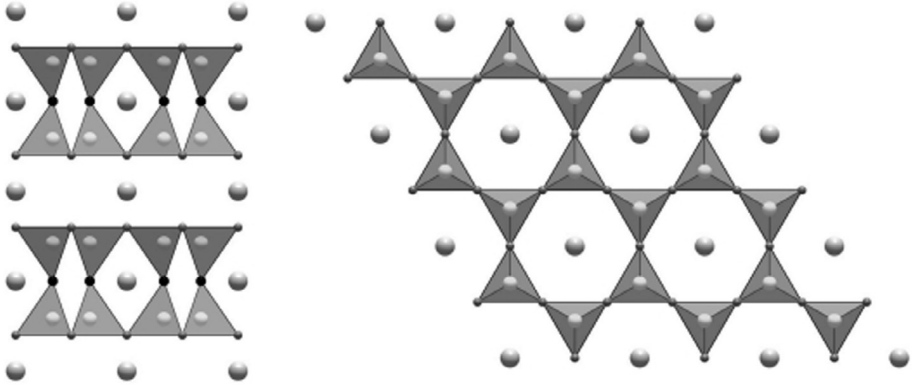

Fig. 4. Left: side view and right: top view of $BaSi_4O_6N_2$, a layered hexacelsian-type structure. Grey triangles represent SiO_3N tetrahedra, with N sitting at the bridging vertex (small black spheres), and larger grey spheres represent Ba^{2+} ions. Reproduced with permission from [40].

Please cite this article in press as: C. Büchner, M. Heyde, Two-dimensional silica opens new perspectives, Prog. Surf. Sci (2017), https://doi.org/10.1016/j.progsurf.2017.09.001

structurally equivalent to silica bilayer films. However, chemically pure SiO_2 hexacelsian structures have not been observed so far. Tetrahedral positions in known hexacelsian minerals are statistically filled with Al or Si atoms, vertices can be formed by O or N, and alkaline or earth alkaline metal ions between the bilayers or inside the hexagonal channels offset the charge imbalance of the aluminosilicate network. It is unclear whether a pure silicate hexacelsian structure can be prepared, from which silica bilayers could be exfoliated on a large scale. If existing hexacelsians allow exfoliation of single layers, they might offer a simple route towards doped 2D silica films.

3. Characterization of pristine silica bilayers

Structural and chemical characterization of silica bilayers has been carried out with a vast array of techniques. We will briefly summarize the reported results, starting from averaging techniques and high resolution microscopy, discussing contributions from vibrational spectroscopy and theoretic modeling, which finally result in a structural model. After discussing the characterization of silica bilayers, we will take a closer look at four research fields that either have received novel impulses from the availability of atomically resolved silica structures, or are likely to benefit in this way from work currently underway.

Low energy electron diffraction (LEED) patterns of silica bilayers represent the variation in the local structure, indicating a (2×2) superstructure for predominantly crystalline films and a ring feature for largely amorphous films. SiO_2 bilayers with roughly equal amounts of crystalline and amorphous domains exhibit LEED patterns with coexisting (2×2) reflexes and ring features [21]. In case of Pd(1 1 1) supports, incommensurate growth of a silica bilayer yields a moiré pattern, and respective satellite spots are visible in LEED [13].

Auger electron spectra (AES) of 2D silica on Ru(0 0 0 1), on Pd(1 0 0) and on Pd(1 1 1) have been reported, showing a main Si peak around 80 eV, and a smaller Si peak at 63 eV [12,13,27,36]. AES signals corresponding to O have been reported between 500 eV and 520 eV [12,27].

XPS has been used to characterize the chemical state and stoichiometry of silica bilayer films on Ru(0 0 0 1) and Pt(1 1 1) substrates with similar results [3,11]. XPS spectra of silica bilayers show one peak for the Si 2p level around 102 eV, which is assigned to Si^{4+} species [3]. No Si^{3+} or Si^{2+} suboxide species have been reported for silica bilayer films, indicating fully oxidized building blocks. The O 1s spectra exhibit a main peak around 531 eV, which is characteristic for Si–O–Si bonds, and a shoulder at roughly 2 eV lower binding energy. The relative intensity of this shoulder signal can vary depending on the film preparation. This energy is in agreement with XPS signals for oxygen adsorbed on ruthenium, and is therefore assigned to the interfacial oxygen coverage, which can be varied without changing the structure of the 2D SiO_2 film [30]. For silica films on Pt (1 1 1), the relative intensity of the interfacial oxygen signal was lower than for Ru(0 0 0 1), which is in agreement with the lower oxygen affinity of platinum compared to ruthenium [11].

He^+ ion scattering spectroscopy was used to compare the surface stoichiometry of predominantly ordered films with that of amorphous films. The spectra showed almost identical intensities for O, Si and Ru, indicating that crystalline and amorphous silica films are chemically equivalent [21].

TPD studies show a clear difference in the CO adsorption of crystalline versus amorphous silica films [21]. Crystalline films show only one desorption feature with low intensity, corresponding to coverages of 1% (meaning 1% of the surface Ru atoms have a CO molecule adsorbed on it). This feature is assigned to defect mediated CO-adsorption, and can also be observed for amorphous bilayers. If the amorphous silica bilayer is prepared in an O-poor configuration, however, additional adsorption sites are made available, resulting in two additional CO desorption features in TPD. These desorption peaks occur at higher temperatures and represent around 5% of the film surface. It is assumed that larger rings in the amorphous network represent such adsorption sites [21].

Scanning tunneling microscopy (STM) and atomic force microscopy (AFM) images reveal films with corrugations of ~20 pm [4], referred to as atomically flat films. The SiO_2 layers closely follow the substrate morphology, and exhibit steps that are consistent in height and orientation with monoatomic terrace steps in the underlying substrate [3,12].

Even when depositing sufficient amounts of Si to cover the substrate surface, mesoscopic holes between 10 and 100 nm in diameter can often be observed in 2D SiO_2 films. These holes expose the underlying, O-covered metal or monolayer patches of silica and are assumed to form during the annealing step. Precise temperature control is required to provide sufficiently high temperatures for complete oxidation, but minimizing dewetting of the silica bilayer films [22].

Based on these holes, different apparent heights from STM measurements have been presented for silica bilayer films. The reported values range from to 3 Å to 5 Å for SiO_2 on Ru(0 0 0 1) [21,36], and 2 Å for SiO_2 on Pt(1 1 1) [11]. When discussing STM-based height values however, a cautious approach should be taken, as the measured apparent height depends on the voltage that is applied and on the respective local densities of state. The different electronic properties of the oxide film, the plain metal substrate/the oxygen covered metal, and the tip material strongly impact the measurement. Only through careful studies and reference measurements can these factors be deconvoluted [44,45]. Another stumbling block is correlating measured values with heights from DFT models. The DFT model for the silica bilayer gives a distance of 4.3 Å between the nuclei of the top- and bottommost O atoms in the film [3]. However, the scanning probe will always detect the local electron density at some distance from the atomic center. Furthermore, when a step height between film and substrate is determined, the van der Waals gap needs to be taken into account. Depending on the adsorbate concentration on the metal, this distance can range from 2.75 Å to 3.85 Å [30]. It is therefore necessary to report apparent heights with a complete set of mea-

Please cite this article in press as: C. Büchner, M. Heyde, Two-dimensional silica opens new perspectives, Prog. Surf. Sci (2017), https://doi.org/10.1016/j.progsurf.2017.09.001

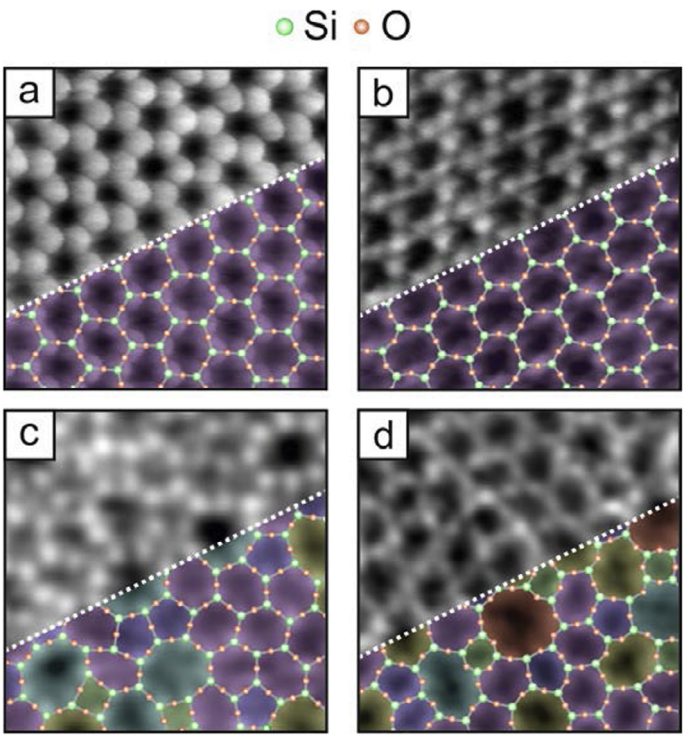

Fig. 5. Atomic resolution STM images of silica bilayers, all scan frames 3.5 nm × 3.5 nm. a) Crystalline bilayer with visible Si atomic positions, V_S = 3 V, I_T = 100 pA. b) Crystalline bilayer with visible O atomic positions, V_S = 0.1 V, I_T = 100 pA. c) Amorphous bilayer with visible Si atomic positions, V_S = 2 V, I_T = 50 pA. d) Amorphous bilayer with visible O atomic positions, V_S = 0.1 V, I_T = 100 pA. Adapted with permission from [46].

surement parameters, including the material of the tip. When comparing relative values of apparent height, these experimental conditions should be specifically addressed.

High resolution STM and AFM images reveal the atomic positions of either O or Si atoms, depending on the tip configuration [46]. Sets of four Si atoms are arranged in windmill-like shapes with Si-Si distances of 3.01 Å to 3.15 Å as shown in Fig. 5a. A different contrast reveals O atomic positions, which are arranged in sets of three, see Fig. 5b. Based on STM images, O–O distances from 2.59 Å to 2.72 Å with standard deviations of 0.2 Å have been reported, which agrees with the value of 2.65 Å, established by ND and XRD experiments. The uncertainty reflects the relatively small number of positions that are considered (in comparison to bulk silica measurements), as well as some uncertainty in the process of coordinate extraction [46]. Both Fig. 5a and b exhibit a periodic arrangement of the small building unit in a honeycomb lattice. This arrangement is referred to as crystalline 2D SiO_2.

The Si-contrast and the O-contrast have also been observed for amorphous silica bilayers (also referred to as vitreous silica), as shown in Fig. 5c and d [46]. Combining both contrasts by placing a Si atom in the center of each O triangle, yields a complete set of atomic coordinates for the top layer of the film. The observed triangular [SiO_3]-building block is one face of the [SiO_4] tetrahedra that form this film system [4].

The in-plane bonds between tetrahedra can assume different angles. Si–Si–Si angles of 120.2 ± 6.3° yield a hexagonal honeycomb lattice with the exact periodicity depending on the substrate. Reported values for lattice constants on different substrates are presented in Table 1. Si–Si–Si angles of 120.2 ± 14.7° have been measured for amorphous networks, forming different rings. Ring sizes range from four- to nine-membered, as indicated with different colors in Fig. 5c and d. Ordered and amorphous domains are often found on the same sample, which also allows the investigation of the phase boundary between amorphous and crystalline regions [24].

These structures have also been observed for a silica film supported on graphene using scanning transmission electron microscopy (STEM) [16]. Annular-dark field STEM images clearly show bright spots that are assigned to Si positions and slightly increased signal intensity between those positions, which is assigned to the O atoms. Electron energy loss spectroscopy (EELS) fine structure measurements indicate the presence of [SiO_4] building blocks [15,16]. The coexistence of crystalline and amorphous structures has been corroborated as well by STEM data.

Another important contribution for the structure model of silica bilayers is provided by infrared reflection absorption spectroscopy (IRAS). A typical spectrum showing two clear absorption bands and schematics of the molecular vibrations involved is presented in Fig. 6. DFT calculations using a bilayer model can quantitatively reproduce the vibrational features.

Please cite this article in press as: C. Büchner, M. Heyde, Two-dimensional silica opens new perspectives, Prog. Surf. Sci (2017), https://doi.org/10.1016/j.progsurf.2017.09.001

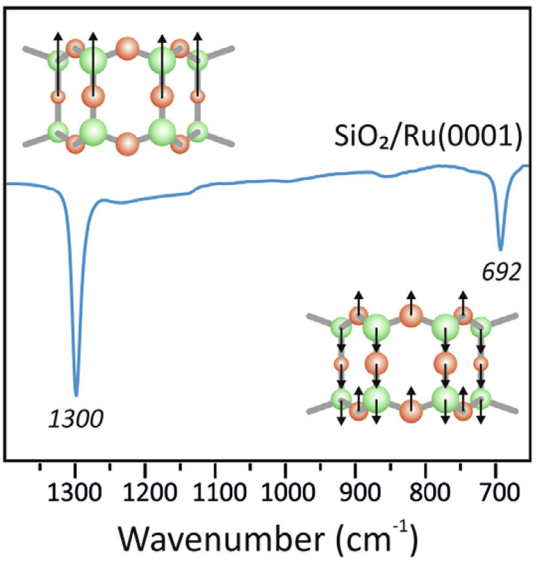

Fig. 6. IR spectrum of silica bilayer on Ru(0 0 0 1), showing the two characteristic signals and the corresponding molecular vibrations as schematic. Adapted from [1]

The main IRAS feature is an absorption band around 1300 cm^{-1} that corresponds to the vibration of Si–O–Si bridges [3]. Due to metal surface selection rules dominating the signal intensity, the vibration at 1300 cm^{-1} is assigned to Si–O–Si groups vibrating perpendicular to the surface. Therefore, the vibrational signature clearly indicates a bilayer structure, where two sheets of building blocks are arranged on the metal substrate, resulting in a Si–O–Si group being oriented perpendicular to the surface. A second characteristic signal in IR spectra is observed around 692 cm^{-1}, indicating an out-of-plane vibration of the Si–O–Si bonds positioned parallel to the surface. Recently, a study of 2D silica signatures in Raman spectroscopy was presented [47], providing a means of fast characterization of silica bilayers, as is needed for large-scale production. The measured spectrum containing five identifiable Raman features is shown in Fig. 7a, and the DFT-based density of states including the two major IR-active modes is presented in Fig. 7b.

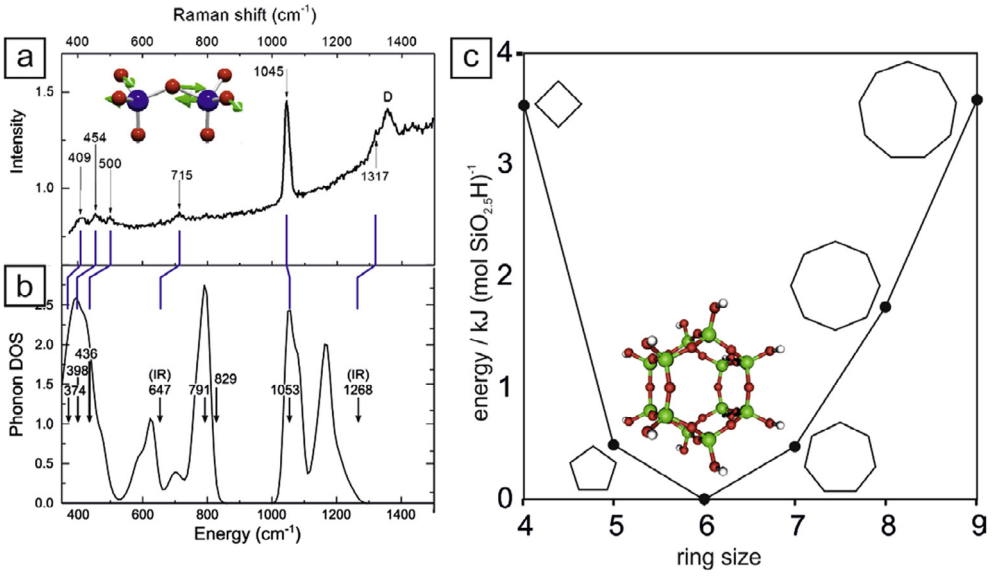

Fig. 7. a) measured Raman spectrum of a 2D silica film. b) calculated phonon density of states including IR active vibrational modes. (Reproduced with permission from [47]) c) Relative energies of different ring sizes, based on DFT models for isolated, hydroxylated double rings, as shown for the case of a six-membered ring. Reproduced with permission from [4].

Theoretical structure models have been developed in tandem with experiments. DFT calculations confirm the energetic feasibility of a hexagonal silica bilayer structure [3], indicating that the interaction with a substrate substantially stabilizes the film [16]. In the best model, each tetrahedron is connected via three O vertices in plane, while the fourth oxygen bridge connects to a tetrahedron in the other layer of the bilayer structure. The bridging oxygen positions form a mirror plane, cutting through the bilayer. These structural features are reflected in scanning probe microscopy (SPM) data and IRAS spectra, and can be reconciled with all other experimental evidence.

Note that due to this mirror plane cutting through the oxygen bridges, silica bilayers are considered highly ordered in the z-direction (parallel to the oxygen bridges), regardless of whether the xy-plane (image plane in SPM) exhibits crystalline or amorphous morphology.

The combination of XPS, IRAS and DFT is also crucial to understanding the role of interfacial oxygen, which can form an ordered adlayer between the metal and the silica film. Before depositing Si in the film preparation, the Ru(0 0 0 1) is covered with oxygen. Depending on the preparation details, a (2×1)O-Ru(0 0 0 1) or a (2×2)3O-Ru(0 0 0 1) surface has been reported, the latter called an O-rich film [3,4]. DFT models show that SiO_2 bilayers on Ru(0 0 0 1) are stable with zero (called O-poor films), two, four, six or eight O-atoms at the interface per (2×2) unit cell. The interfacial oxygen can be reversibly removed and replaced by heating the system in UHV or in oxygen partial pressure, respectively [30]. This process does not significantly affect the film structure. The presence of adsorbed oxygen can be detected as a shoulder in the O1s signal in XPS. The energy of this shoulder is in good agreement with O adsorbed on plain Ru(0 0 0 1), while the intensity correlates with the oxygen coverage [3]. This shoulder signal is significantly weaker for silica films grown on Pt(1 1 1), which has a lower oxygen affinity [11].

For 2D silica grown on Pd(1 0 0), the presence of a well-ordered interfacial oxygen layer has been ruled out, considering the incommensurability of the Pd-lattice, the hexagonal silica lattice and a possible (2×2) oxygen lattice [12]. The silica films grown in solid state growth methods were not annealed in an oxygen partial pressure [15,16]. Extrapolating from the UHV-annealed films on ruthenium, which tend to form the O-poor system, we can assume that the solid-state grown films have no interfacial oxygen.

The network structures of silica bilayers seem largely unaffected by the presence or absence of an underlying oxygen layer. However, the interfacial oxygen plays an important role for the adsorption properties of the system, which will be further addressed in Section 4. Furthermore, adsorbed oxygen influences the overall work function, which is discussed below with other electronic properties.

The electronic properties of silica bilayers have been investigated to a lesser extent that their atomic structure, and some aspects of the electronic structure have not been addressed to far. Employing scanning probe assisted methods, the work function and band gap of silica bilayers have been studied early on.

By sweeping the bias between STM tip and sample, field emission resonance spectra can be obtained. Extracting the energetic onset of the resonances gives insight into the material's work function. Using this method, it was found that the preparation of a silica monolayer on Ru(0 0 0 1) lowers the system's work function from initially 5.5 eV to 4.65 eV. The bilayer preparation on the other hand, gives a work function value of 5.5 eV. Therefore, the work function difference between the monolayer and the bilayer system is 0.85 eV [48].

This value can be compared against the local contact potential, which was determined with a Kelvin probe measurement using the AFM sensor [49]. This measurement does not give the absolute work function, but by measuring a monolayer film and a bilayer on the same substrate with the same setup, the work function change can be obtained. Based on this approach, the work function of a silica bilayer on Ru is 0.07 eV higher than that of a monolayer [48]. However, more experiments are needed to understand the electronic properties relevant to catalytic and nanoelectronic applications. Mapping the work function differences on crystalline and amorphous films, as well as on defect sites and different building blocks with high local resolution would allow understanding the contact potential variations within the tetrahedral network, which determines reactivity and transport properties.

Other components of the thin film system are also known to influence the work function. In an XPS study, the removal of the oxygen adsorbate layer was found to lower the overall work function by 0.8 eV [50]. This was corroborated in a study investigating different O-coverages underneath a silica bilayer, which reported a slightly larger work function decrease of 0.95 eV for the complete removal of interfacial oxygen [51]. XPS was also used to investigate the adsorption of Pd and Au atoms, which are preferentially located at the film-substrate interface. It was observed that adsorbed Pd or Au atoms decrease the system's work function by up to 1.2 eV, correlating with the coverage amount [50]. Corresponding DFT calculations show that electrons are transferred from the adatoms to the substrate, which explains the macroscopic work function reduction. Similar effects are predicted for the adsorption of Na or Mg. The respective work function decreases are predicted to be at least 1 eV, and substantially more if the positive adatoms are located on top of the film surface [52]. Hence, metal atom adsorption introduces reactive sites into the otherwise inert silica film. The influence of those dopants that are covalently bound in the film structure has not been determined so far. It is however expected that replacing a number of Si network nodes with Al atoms would alter the electronic properties.

The local density of states can also be probed with an STM tip, which allows extracting a value for the band gap of the film. For a SiO_2 bilayer on Ru(0 0 0 1), a value of 6.5 eV was determined, which is slightly lower than the value of 6.7 eV obtained for the monolayer [48]. Several DFT studies report densities of state, from which a band gap might be derived. Calculations from different groups using a generalized gradient approximation find values between 4.5 eV and 5.73 eV [16,25,50]. A comparison of a fully hexagonal bilayer and a so-called haeckelite bilayer (comprised of only five- and seven-membered rings)

Please cite this article in press as: C. Büchner, M. Heyde, Two-dimensional silica opens new perspectives, Prog. Surf. Sci (2017), https://doi.org/10.1016/j.progsurf.2017.09.001

shows a slight change in the respective work function [25]. The same study also used a hybrid HSE06 functional, which is more suitable for estimating band gaps. This treatment yields a band gap of up to 7.2 eV for the silica bilayer [25].

Complete band structure measurements of silica bilayers, including the role of the oxygen adsorbate layer, are of interest to characterize this material further. The atomic-level structural characterization, coupled with band structure studies, may yield new insights into band structures of disordered solids.

In order to model amorphous systems, DFT models of extended defect structures can be created. Starting from a hexagonal bilayer, a model defect can be created by rotating a Si–O–Si bond by 90°. This operation yields a Stone-Wales type defect, consisting of two five-membered rings and two seven-membered rings. By repeating this step, DFT models of amorphous silica bilayers can be obtained. The energy difference between ordered and disordered silica bilayers was found to be lower than the typical energy difference between crystalline and vitreous bulk silica [4]. Hence, amorphous 2D SiO_2 films are concluded to be metastable. The relative energy for differently sized rings was determined for isolated double rings saturated with OH-groups, shown in Fig. 7c [4]. These relative energies roughly correlate with the observed distribution of ring sizes, indicating that the six-membered ring is the most stable species, and that five- and seven-membered rings, eight-membered rings and four-and nine-membered rings are successively higher in energy [4].

3.1. Impact of real-space data on amorphous network structures

The surface structure of silica has been studied for decades, in crystalline and amorphous forms. Due to its surface roughness and insulating nature, amorphous SiO_2 is an especially challenging material for many surface science methods, as they often rely on charge transport. 2D silica films are atomically flat and allow the unhampered investigation of this electrical insulator with surface science. High resolution microscopy has revealed the atomic structure of these films, which is particularly insightful in case of defect-rich and amorphous silica films. The availability of these data has implications for several distinct research topics, which we will discuss briefly. We will leave all matters relating catalysis for Section 4, where we deal with chemical modifications to silica films, which in turn affect the reactivity.

3.2. Obtaining locally resolved information on defect structures

Defect structures such as coordination defects, packing defects and grain boundaries represent a deviation from the perfect crystal structure. Historically, experimental techniques for studying atomic structures have relied on integrating a signal over many atomic positions in a crystal. Through this approach, X-ray diffraction (XRD), neutron diffraction (ND) and nuclear magnetic resonance spectroscopy (NMR) contributed to the discovery of many structures. Rare and isolated defect sites, however, give only weak signal contributions in these techniques, and materials without long-range order produce broad signals that defy unambiguous assignments.

Microscopy can provide information in real space, and hence address local defects with high resolution. Rough surfaces have previously impeded the interpretation of microscopy data from glass samples [53,54]. This challenge is overcome with the creation of a thin film system that reproduces the flatness of its single crystal substrate. Hence, a defect-rich silica system is accessible for real-space techniques. Understanding what drives the formation of defects and how they affect material properties is the basis for developing custom-tailored thin films.

In this section, we will consider *structural defects* of crystalline silica bilayers, where elements deviating from the ordered honeycomb lattice are observed. This is to be distinguished from *coordinative defects*, like under- or over-coordinated atoms, which are not observed in continuous silica bilayers.

Crystalline SiO_2 bilayer films can exhibit different point defects and line defects, which were imaged with atomic resolution. Several structure motifs that are observed in silica layers can also be found in other honeycomb networks. Fig. 8a–d shows models of different point defects (top row), which have been observed in silica layers (data from STEM shown in middle row) and in graphene sheets (bottom row). Note the different length scales for the two networks; one edge in the model represents the Si–O–Si moiety for the SiO_2 bilayer, but a C–C bond with roughly half the length in case of the graphene monolayer. All the point defects shown in this figure exclusively consist of five-, six- and seven-membered rings. The defect shown in Fig. 8a, formed by two seven-membered and two five-membered rings, is known as the Stone Wales defect and occurs frequently in hexagonal systems [55–57]. Starting from a honeycomb lattice, the Stone Wales defect can be created conceptually, via rotating one Si–O–Si group per layer by 90 degrees. Bond excitation through an electron beam in STEM experiments has been employed to create and to annihilate Stone-Wales defects in silica bilayers [58,59], but some details of the defect formation mechanism remain to be resolved further. The defect shown in Fig. 8b possesses the shape of a flower, and consists of a microcrystallite domain in the center that is rotated by 30° with respect to the orientation of the main lattice, separated by a boundary of five- and seven-membered rings.

Both the Stone-Wales and the flower defect have the same atom density as the ordered lattice, and can be formed by simple bond rearrangements. These kinds of defects are topological defects [58]. The divacancy defect shown in Fig. 8c, however, has a lower density compared to the surrounding lattice, while the cross-shaped defect in Fig. 8d shows a higher density than the surrounding sheet. The formation of these defects includes addition or removal of atoms.

Several kinds of line defects have been reported for silica bilayers, typically labelled as grain boundary or domain boundary. Grain boundaries can best be classified by the ring sizes that are incorporated in it and their orientation with respect to

Please cite this article in press as: C. Büchner, M. Heyde, Two-dimensional silica opens new perspectives, Prog. Surf. Sci (2017), https://doi.org/10.1016/j.progsurf.2017.09.001

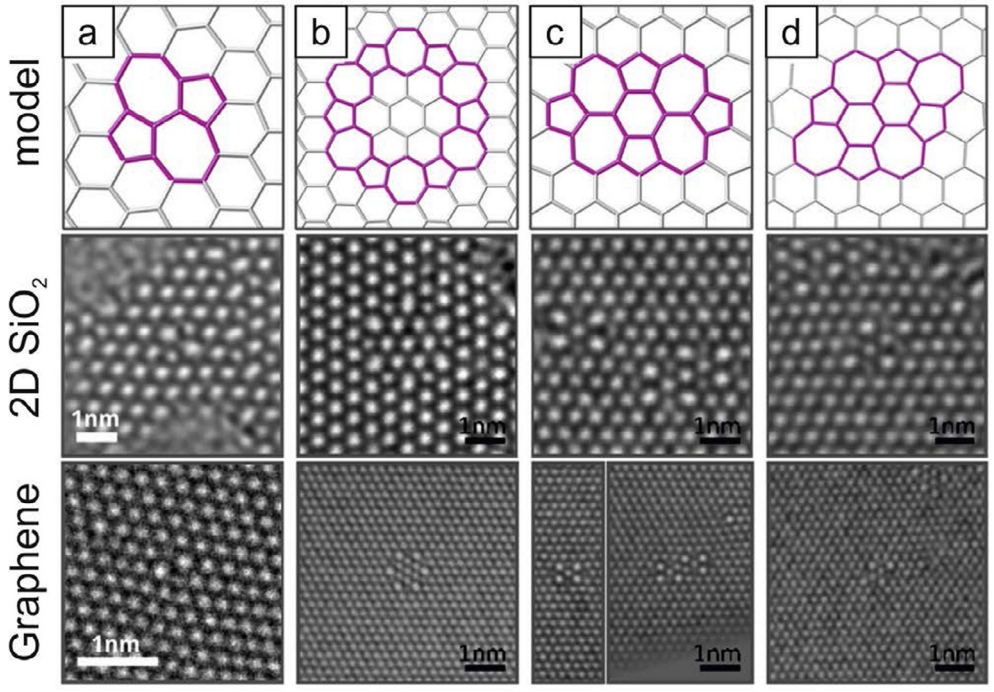

Fig. 8. Point defects in hexagonal networks. Models (top row) and TEM images of different point defects in hexagonal networks, observed in silica bilayers supported on graphene (middle row) and graphene (bottom row), respectively. a) Stone-Wales defect, b) flower defect, c) double vacancy d) cross-shaped defect with additional atoms. Reproduced with permission from [58].

the metal substrate. Fig. 9a shows an STM image of a crystalline silica bilayer on Ru(0 0 0 1) with three grain boundaries intersecting in the lower half of the image [60]. Two of those grain boundaries consist of alternating five- and seven-membered rings and are found with many different orientations on the substrate. For short, we will call these structure elements *57-boundaries*, and label other line defects accordingly. 57-boundaries typically separate two hexagonal domains which are rotated by 30° [60]. The point defects shown in Fig. 8 can be considered closed-loop versions of the 57-boundary as well. Except for the Stone-Wales defect, all these point defects contain one or several hexagons, which are rotated by 30° with respect to the surrounding crystalline domain. A TEM study of 2D SiO_2 on graphene reported a similar network of meandering grain boundaries consisting of five- and seven-membered rings [16,58].

On the lower left-hand corner of Fig. 9a, a straight domain boundary is shown, consisting of two five-membered rings and one eight-membered ring as the repeating element. For SiO_2 bilayers on Ru(0 0 0 1), this is the most frequently observed type of domain boundary [60]. It is found to separate grains of crystalline SiO_2, which exhibit the same orientation but are offset by one Ru(0 0 0 1) lattice constant. 558-boundaries are observed only in the [1 0 0 0] direction of the Ru substrate, or rotated by 60° or 120°, respectively.

In rare cases, domain boundaries formed by alternating four- and eight-membered rings or more complex ring arrangements between grains are observed in crystalline silica bilayers on Ru(0 0 0 1) [60].

For 2D SiO_2 on Pd(1 0 0), an array of antiphase domain boundaries has been observed, that preferentially run across the crystal direction of the silica network, with an elongated unit cell in the Pd [0 $\bar{1}$ 1] direction [12]. Fig. 9b shows a high resolution STM of the SiO_2 film, indicating the domain boundaries with white arrows. The structure model for this type of boundary is presented in Fig. 9c, consisting of elongated eight-membered rings, separating two hexagonal domains with the same orientation and offset by one substrate lattice constant. A side view of the domain boundary in Fig. 9d shows that the Si position situated in the middle of the boundary is bridged via two oxygen atoms to the Si atom below. As a consequence the silica film contains highly strained two-membered rings, but it is stoichiometrically still SiO_2.

Atomically resolved data on ordered and amorphous SiO_2 bilayers allows studying the similarities that defects in the ordered phase exhibit in comparison to amorphous networks [60]. One common concept of amorphous structures assumes that they are merely the spatially extended version of local defects, which have been studied for many decades [61]. It was found however, while the topological transition from a honeycomb lattice to a disordered network gradually introduces ring size variations [24], domain boundaries in crystalline SiO_2 abruptly exhibit very strained ring sizes directly interfacing the crystalline phase [60]. Hence, domain boundaries are unlikely precursors for the amorphous

Please cite this article in press as: C. Büchner, M. Heyde, Two-dimensional silica opens new perspectives, Prog. Surf. Sci (2017), https://doi.org/10.1016/j.progsurf.2017.09.001

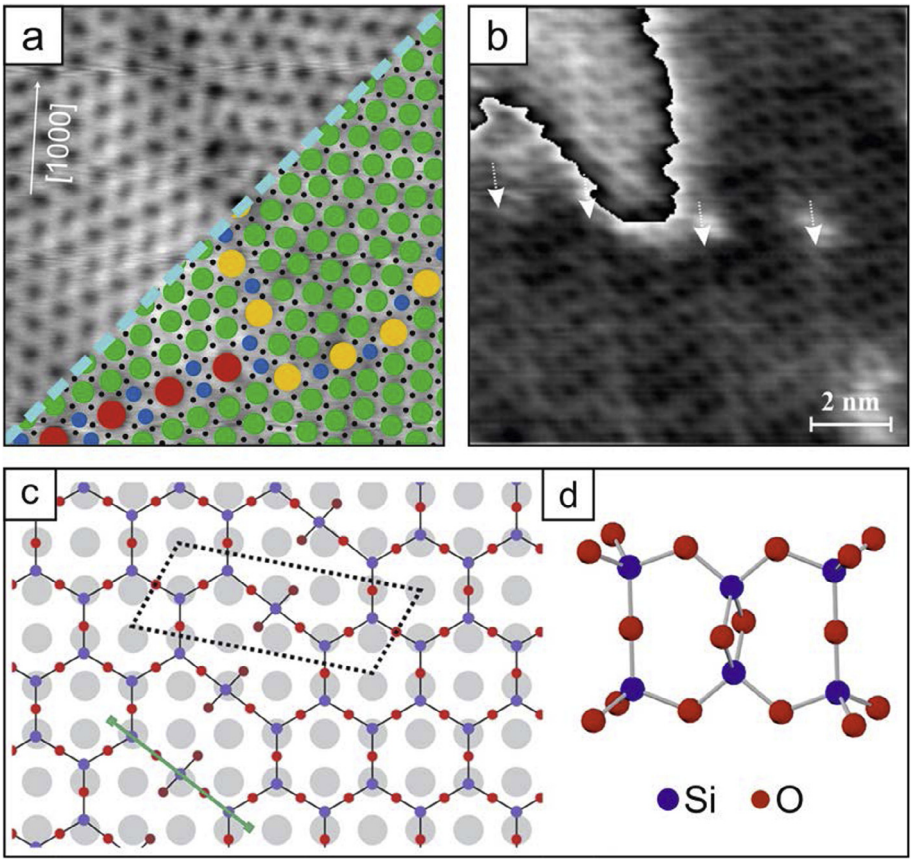

Fig. 9. Grain boundaries in crystalline 2D SiO_2 films. a) Crystalline 2D SiO_2/Ru(0 0 0 1), exhibiting two 57-domain boundaries and a 558-domain boundary. On the lower half of the image, Si positions are marked with black circles, and color-coded disks mark the structure model. Scan area 7.4 nm × 7.4 nm, V_S = 0.5 V, I_T = 100 pA, adapted with permission from [60]. b) Crystalline 2D SiO_2/Pd(1 0 0), exhibiting antiphase domain boundaries. White arrows indicate the boundaries. The grey scale for this STM was cycled through twice to show the contrast on the upper and lower terrace, V_S = 0.5 V. c) Structural model of crystalline 2D SiO_2/Pd(1 0 0), exhibiting a domain boundary consisting of 8-membered rings in the imaging plane. d) Side view of the structure element of the domain boundary, exhibiting two-membered rings connecting the top and bottom layer. Panels b)- d) reproduced with permission from [12].

phase. All observed line defects were also highly periodic in their ring arrangement, while amorphous regions do not show any periodicity.

In graphene and 2D semiconductor materials, defects crucially influence mechanical and electronic properties, and have considerable impact on the ability to use the respective 2D material in technological applications [62]. Depending on the intended use, controlling the occurrence and morphology of defects can be an objective, also known as defect engineering, but avoiding defects altogether is the common goal of many studies. A DFT study suggested that tuning defects in SiO_2 through preparation conditions may be possible by choosing substrates that provide the right amount of epitaxial strain. Due to the strain, ring motifs other than hexagons are lowered energetically, and therefore various domain boundary structures may be created with suitable substrates [26]. Conversely, choosing a low-mismatch substrate should help minimize line defects. This approach was successfully demonstrated by custom-tailoring the lattice constant of a metal thin film substrate. By preparing 2D silica on a 48% Ni and 52% Pd alloy thin film, epitaxial strain was minimized, and the resulting films exhibit a sharp (2 × 2) LEED pattern. In STM, no line defects and no amorphous regions have been observed, indicating a 'zero-strain' system [14].

Only few experimental studies have investigated the material properties resulting from the presence of point and line defects in silica bilayer films. Structural defects have been considered as potential reactive sites for hydroxylation, but coordinative defects such as atomic positions at step edges are assumed to be more reactive [63].

As line defects in 2D SiO_2 consist of ring sizes other than the hexagons that form the crystalline lattice, they provide larger pore sizes for atomic or molecular species to penetrate the oxide film. This property has been used for adsorption experiments with single Au atoms on defect-rich 2D SiO_2 on Ru(0 0 0 1). Gold atoms are too large to migrate through the six-membered rings of crystalline silica bilayers, but they have been observed to penetrate the 558-domain boundary, most likely diffusing through the eight-membered rings [50].

Please cite this article in press as: C. Büchner, M. Heyde, Two-dimensional silica opens new perspectives, Prog. Surf. Sci (2017), https://doi.org/10.1016/j.progsurf.2017.09.001

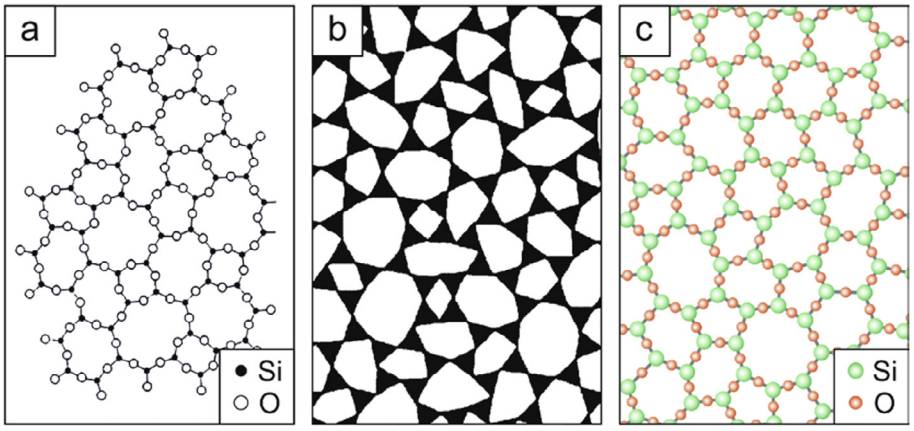

Fig. 10. Models of SiO_2 glass networks. a) Zachariasen model of a continuous random network. Reproduced with permission from [67]. b) Triangle raft by Shackelford, modeling glass networks. Reproduced with permission from [68]. c) Network structure of a SiO_2 bilayer on Ru(0 0 0 1), based on STM data.

3.3. Understanding the nature of the glassy state

In contrast to crystalline materials, which can be described structurally in simple ways, amorphous or glassy materials still hold a few mysteries. No experimental technique is able to provide real space atomic structure data of a bulk glass at this point. For the last century, the main source of insights on glasses were diffraction experiments, which provide information in reciprocal space, averaged over many atomic positions. Due to the lack of periodicity in glasses, diffractograms typically consist of broad signals and are not straightforward to interpret. Instead, model glass structures were developed and their diffraction signature compared to experiments. For a historic overview of modeling approaches for understanding glasses, we recommend a review by A. C. Wright and M. Thorpe [64].

The discovery of atomically flat SiO_2 films allows collecting atomic resolution data of amorphous structures and is therefore an important step in evolving our concept of glassy materials. A prominent feature of the topology images are the ring units formed by several tetrahedral building blocks. The existence of such rings had already been deduced from measurements of the characteristic vibrational modes of bulk silica [65]. Furthermore, distributions of ring sizes had been inferred from measuring silica's permeability for gas species of different sizes [66].

Real space data on the amorphous ring network not only provide direct evidence for the existence of such rings, but can further address their spatial arrangement, providing two-dimensional information which simply cannot be captured in one-dimensional data like pair correlation functions typically extracted from diffraction results.

The structures observed on amorphous silica bilayers have been compared against amorphous structure concepts from literature. The resemblance of the 2D network of rings to Zachariasen's random continuous network is striking, although the original Zachariasen postulate was describing a three-dimensional (3D) network and merely using a two-dimensional illustration shown in Fig. 10a for clarity [4,16,67]. Zachariasen hypothesized that the tetrahedral building unit for crystalline and amorphous analogs of the same compound would be identical. High-resolution STM images of crystalline and amorphous silica bilayers on Ru(0 0 0 1) verified this assumption [46]. It is the connection of two or more [SiO_4] tetrahedra that introduces variation in the connection angles, which allows the formation of different ring sizes.

SiO_2 bilayers on Ru(0 0 0 1), on Pt(1 1 1) and on Pd(1 0 0) contain rings ranging mostly from four- to nine-membered [4,11,23]. Electron microscopy images of 2D SiO_2 on graphene showed rings from three- to ten-membered [16]. Ring

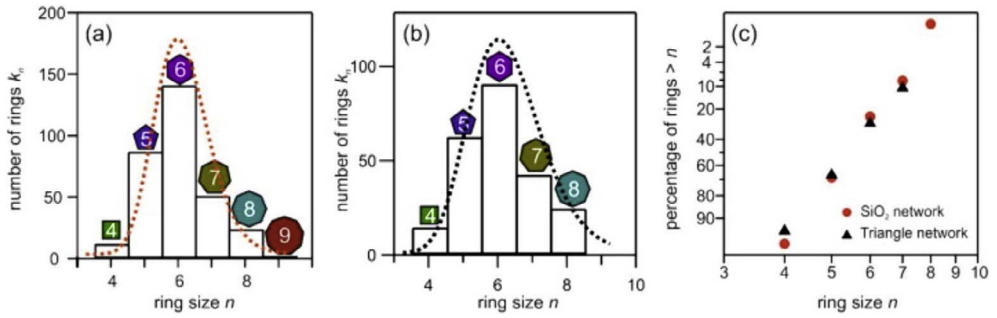

Fig. 11. a) Ring statistic of an amorphous 2D SiO_2/Ru(0 0 0 1) network (317 rings), compared to b) ring statistic from an artificially generated triangle raft structure (237 rings). Both systems exhibit a log-normal ring size distribution, as shown in c). a)-c) reproduced with permission from [69].

statistics for the Ru(0 0 0 1)- and Pd(1 0 0)-supported networks exhibit a lognormal distribution, such as the example shown in Fig. 11a [23,69]. The fact that the ring sizes show a distribution that is asymmetric with respect to the maximum was predicted by Shackelford on the basis of artificially created triangle rafts, shown in Fig. 10b [68,70]. These structures were developed to recreate Zachariasen's two-dimensional illustration by randomly connecting triangular building blocks into a network of rings. The resulting distribution of ring sizes is shown in Fig. 11b. Even though the maximum ring size was limited at eight for the triangle raft, the distributions for both the silica bilayer and the triangle raft follow a similar log-normal distribution, compared in a log-normal probability plot in Fig. 11c [69]. A deviation from this log-normal distribution is predicted for silica networks under large pressures. Molecular dynamics (MD) simulations of these systems observe a widening of the ring size distribution, transitioning into a normal distribution [70].

The reported ring statistics for 2D SiO_2 on graphene deviate somewhat from the distributions for metal-supported silica layers, which can be assigned to a different criterion that was used for selecting amorphous areas [16]. Here, microcrystalline regions of 3×3 hexagons were excluded from the statistics of the amorphous regions, while such a distinction has not been mentioned for metal-supported SiO_2 layers. The different approaches of the respective author teams highlight that the common definition of a crystalline solid exhibits a gap when very short length scales are considered.

The ring size distribution (Fig. 11) observed in SiO_2 bilayers qualitatively reflects the relative formation energies for different ring sizes, as determined by DFT calculations (see Fig. 7c). Atomically resolved images of extended networks, however, provide the opportunity to study larger sheets and identify conditions for the spatial arrangement of different rings. This was done for a network of 317 rings in a silica bilayer on Ru(0 0 0 1) [69], and in a comparative study for several datasets of silica bilayers from experiment and theory [71]. For ring triplets sharing a central Si atom, it was observed that the possible ring combinations are governed by geometrical strain that limits the variation in the tetrahedral angle [69]. As a consequence, the arrangement of rings is not random, but large rings are preferably found next to small rings and vice versa. In particular, the Aboav-Weaire law captures this tendency, which is also found in other cellular networks like biological tissue or condensed droplets [57]. The Aboav-Weaire law predicts the mean size of the distribution of rings that are found adjacent to a particular ring size. In a study comparing silica ring networks from several experimental studies and theoretical amorphous sheets, it was established that the Aboav-Weaire law reflects a seemingly universal topological requirement for 2D amorphous networks [71], providing a good fit for all networks that were studied. However, the (empirically chosen) fitting parameters appear to be unique to each studied network [69,72].

Another morphological descriptor developed from the investigation of cellular networks is Lewis' law, establishing a linear relationship between the vertices in a polygon and its area [72,73]. It was found, however, that Lewis' law is not the best descriptor for the size-area relationship for polygons in the silica network. In the regime of covalent bond networks with little variability in bond lengths, network structures relax into the least distorted ring shapes possible, maximizing ring areas [71].

Developing a better conceptual description for glasses is the motivation for studying successively larger building units of amorphous networks, beyond rings that are directly adjacent. A recent study explored the ring correlations of an extended theoretical network of ~50,000 rings [74], determining over which lateral distances ring sizes show any size correlation. It was found that analyzing the ring network under the criterion of topological distances led to artifacts of long-range correlations, while analyses based on the simple geometric distance showed that correlations cease across roughly three ring diameters [74].

Such insights on how to best analyze and describe amorphous networks can potentially be transferred to other disordered and defect-rich systems. A study compared the respective pair distance histograms and ring size distributions of several two-dimensional structures, shown in Figs. 12 and 13 [55,75]. The selection for this cross-system comparison includes ordered and disordered systems, as well as covalently bound and macroscopic systems, all of which have a threefold connectivity for each building block, and for which high resolution images or 2D structure data was available at the time. The panels in Fig. 12 show a) the model of a 7×7 reconstruction of a Si(1 1 1) surface [76], b) an STM image of a crystalline SiO_2 bilayer on Ru (0 0 0 1) [46], c) an STM image of an amorphous SiO_2 bilayer on Ru(0 0 0 1) [55], d) a DFT model of amorphous graphene [77], while Fig. 13 shows e) an STM of a metastable, defect-rich Cu_2O (1 1 1) surface [78], f) an STM of polymerized 1,3,5-tris(4-bromophenyl) benzene (TBPB) on Au(1 1 1) [79], g) a computational triangle raft [70], and h) a macroscopic bubble raft [55], and the respective ring size histogram.

It was found that the pair distance histograms for all tetrahedral networks show good agreement. Regarding ring sizes, some differences are observed. A convenient way to compare the distributions of different ring sizes is to plot their respective probability against a logarithmic scale, shown in Fig. 14. Based on the studies on triangle rafts, Shackelford proposed that all 2D amorphous networks should adhere to a log-normal distribution, which gives a linear behavior in this plot [70]. It was found that the amorphous systems with covalent bonds indeed adhere to a log-normal distribution. This observation is assigned to the rigidity of the bond lengths and angles, which constrain the tiling of the 2D plane with certain ring sizes. This limitation does not exist for the network of soap bubbles. Hence, the ring size distribution has a greater degree of flexibility and cannot be described suitably by a log-normal distribution. Furthermore, the Si (7×7) reconstruction exhibits a distribution of different ring sizes, but is highly ordered. Its ring sizes do not follow a log-normal distribution, as seen in Fig. 14. Understanding the structure formation of silica bilayers may be applicable to other bilayer systems and materials with double ring motifs, such as zeolite secondary building units (SBUs) [80], water bilayers [81], or double cages in carbohydrates.

Please cite this article in press as: C. Büchner, M. Heyde, Two-dimensional silica opens new perspectives, Prog. Surf. Sci (2017), https://doi.org/10.1016/j.progsurf.2017.09.001

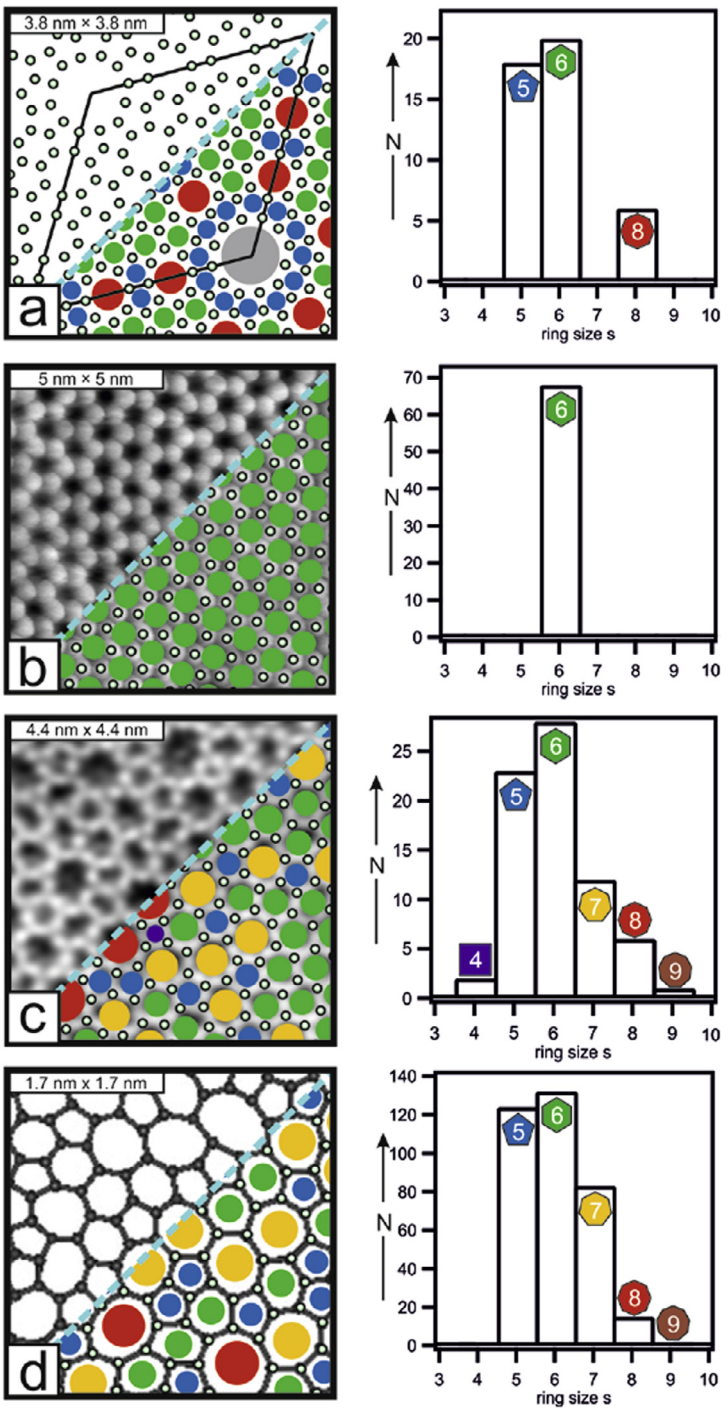

Fig. 12. Comparing real-space structures of 2D tetrahedral networks. Connection points are marked with small green spheres and different ring sizes are marked with color-coded disks. a) Model of a Si(1 1 1) surface in the 7 × 7 reconstruction. The corresponding ring size histogram shows five-, six-, and eight-membered rings. b) STM of crystalline SiO_2 bilayer. Only six-membered rings occur. c) STM of amorphous SiO_2 bilayer. Ring sizes from four to nine are observed. d) DFT model of amorphous graphene, exhibiting ring sizes from five to nine. Reproduced with permission from [75]. (For interpretation of the references to color in this figure legend, the reader is referred to the web version of this article.)

In discussing order and disorder, crystals and amorphous materials, cross-referencing the properties of quasicrystals can be enlightening. The discovery of quasicrystalline systems has reshaped our understanding of crystallinity [82,83]. Although most quasicrystalline structures have been reported for metal alloys, also other material classes form quasicrystals. Recently, thin film quasicrystalline systems have become available for an oxide and a self-assembled molecule network [84,85]. Thus,

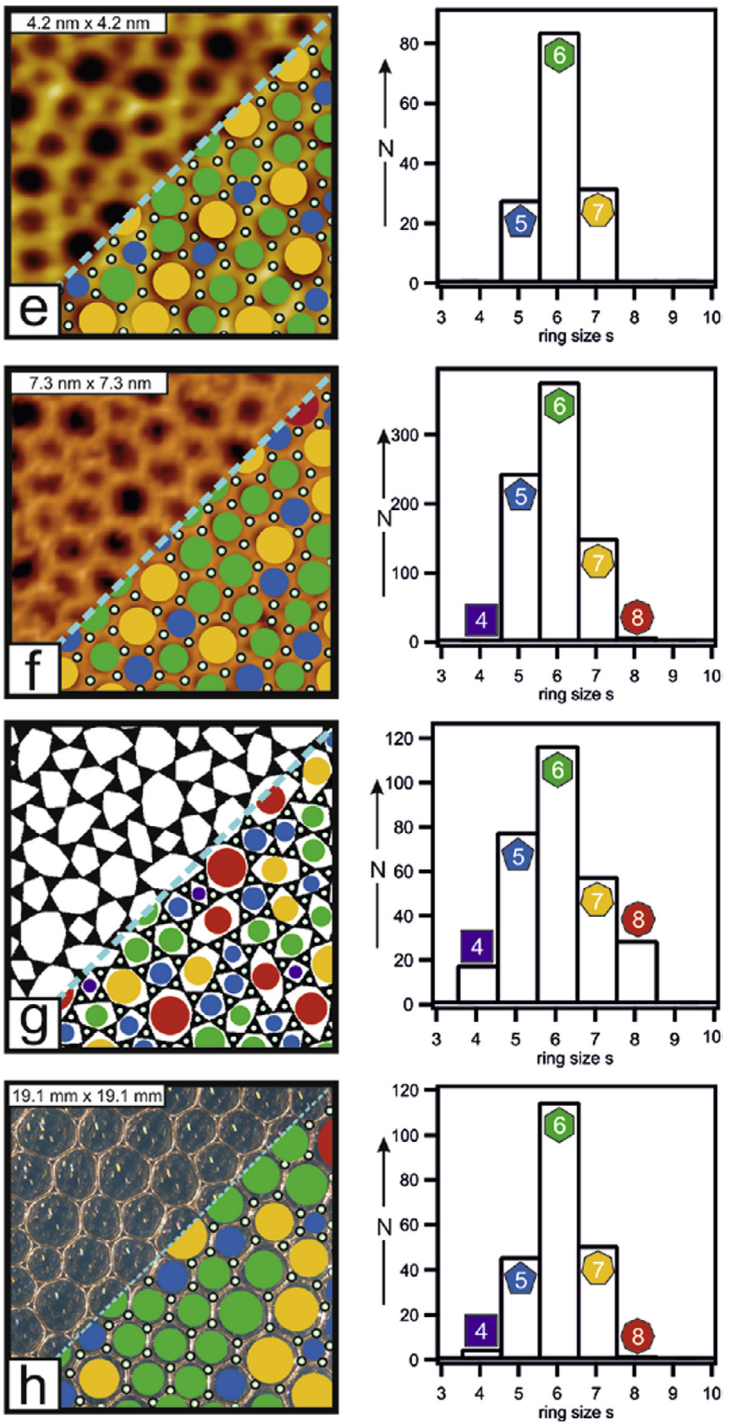

Fig. 13. Comparing real-space structures of 2D tetrahedral networks (continued). Connection points are marked with small green spheres and different ring sizes are marked with color-coded disks. e) STM of defect-rich $Cu_2O(1\,1\,1)$. The ring size histogram shows ring sizes from five- to seven-membered. f) STM of polymerized TBPB on Au(1 1 1), forming four- to eight-membered rings. g) Triangle raft. The ring size histogram shows four- to eight-membered rings. h) Macroscopic bubble raft. Four- to eight-membered rings are observed. Reproduced with permission from [75]. (For interpretation of the references to color in this figure legend, the reader is referred to the web version of this article.)

a comparison of structures can be drawn immediately, considering only the surface plane and discussing the building blocks on the basis of STM images. The quasicrystal networks contain a discrete number of secondary building units, with fixed geometries. Both a quasicrystalline $BaTiO_3$ thin film grown on Pt(1 1 1) and a 2D metal organic framework on Au(1 1 1)

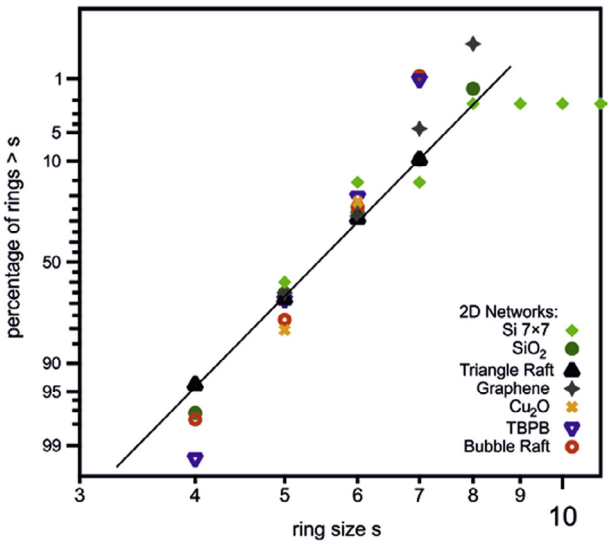

Fig. 14. Log-normal probability plot for ring size distributions of 2D networks referenced in Figs. 12 and 13. The crystalline silica network exhibits only one ring size and is not represented in this diagram. The black line is a guide to the eye, marking a possible linear progression. The Si (7×7) reconstruction deviates clearly from a linear behavior. Reproduced with permission from [75].

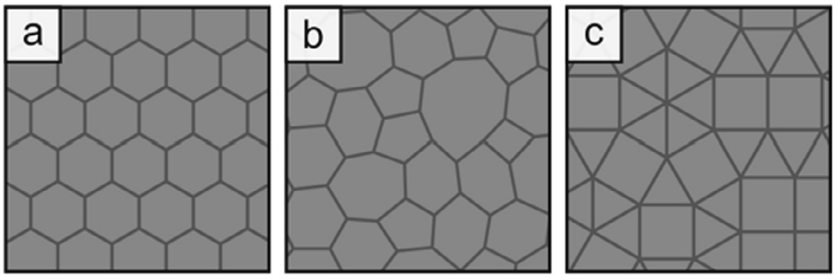

Fig. 15. Schematic of two-dimensional crystal, amorphous network, and quasi-crystal. a) Ordered honeycomb lattice, exhibiting long-range order and periodicity with a constant coordination number. b) Amorphous network without long-range order or periodicity, but a constant coordination number. c) Quasicrystalline network, exhibiting long-range order, but no periodicity and varying coordination numbers.

consist of quadratic and triangular tiles filling 2D space [84,85]. The squares and triangles are highly symmetric and have fixed internal angles.

Conversely, 2D silica exhibits more flexibility in its bond angles, connecting tetrahedral building units to various ring sizes, including distorted rings. When the structural building units are connected with regular angles, an ordered lattice with long range order and periodicity is the result, shown schematically in Fig. 15a. In amorphous silica, the 2D space can be fully covered with the secondary building units, with rings stretching or compressing to fit together, shown in Fig. 15b. In both crystalline and amorphous 2D SiO_2, the coordination number is constant. In quasicrystals on the other hand, the space filling problem is solved by varying the coordination number of the rigid tiles, visible in Fig. 15c. Both amorphous networks and quasicrystals lack long range periodicity, but the latter exhibit long-range order. For both the amorphous and the quasicrystal thin film models, it is surprising that it is possible to grow an ultrathin, aperiodic system on single crystal substrates, which should provide a strong drive towards highly ordered structures.

The ability to manipulate the structure of silica bilayers, coupled with the availability of atomically resolved data, also sheds light on the process of glass transition, which at this point is still not fully understood. Due to the coexistence of crystalline and amorphous domains in many silica film preparations, the structural relationship between the crystal and the glass was thoroughly described based on STM data [24]. A 2D SiO_2 layer was imaged with atomic resolution, revealing a crystalline-amorphous interface. In the transition region, the chemical coordination of all positions is constant, without over- or undercoordination. Adjacent to the crystalline phase, only five-, six- and seven-membered rings were observed, while other ring sizes were not observed directly at the interface, but only occurred deeper into the amorphous region [24]. By defining and tracking a crystallinity value across different regions of the image, the transition from a fully crystalline to a prototypical amorphous region is captured quantitatively, including defining a transition width. For the silica bilayer, the transition region was found to be 1.6 nm wide. These observations are reproduced qualitatively by a crystalline-amorphous

Please cite this article in press as: C. Büchner, M. Heyde, Two-dimensional silica opens new perspectives, Prog. Surf. Sci (2017), https://doi.org/10.1016/j.progsurf.2017.09.001

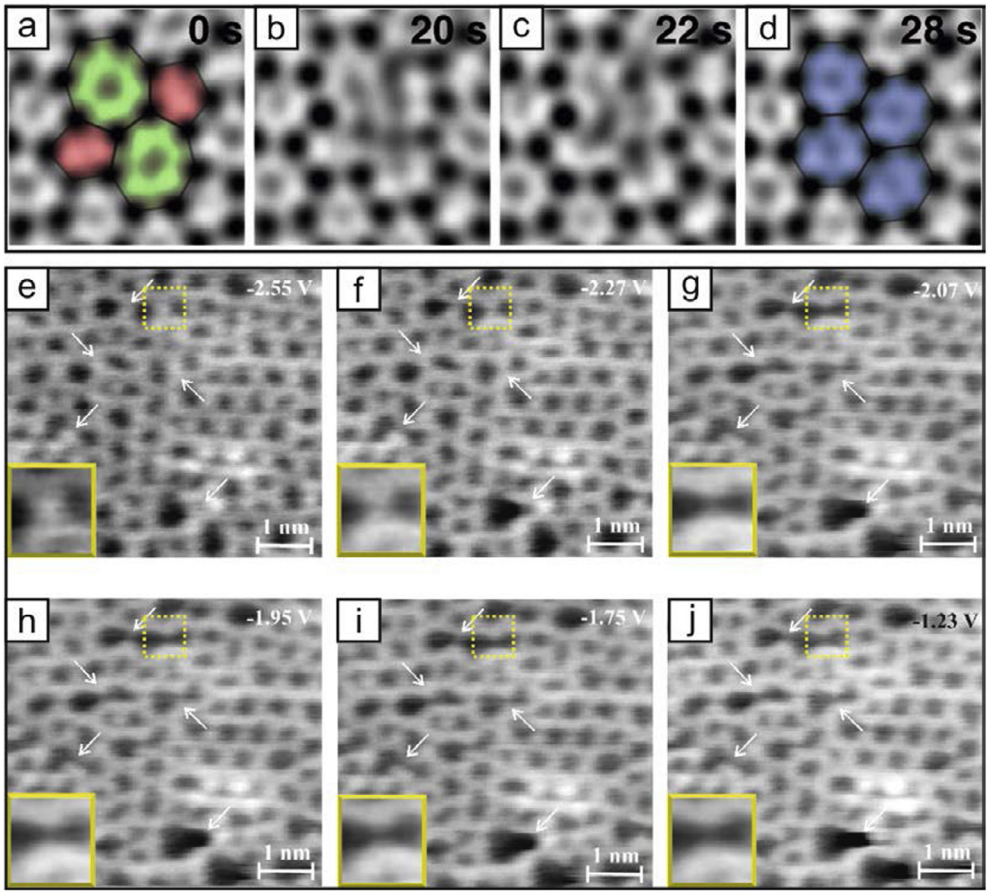

Fig. 16. a-d) STEM images showing a dynamic ring rearrangement from a 5775-cluster to a 6666-cluster, excited by the imaging electron beam. Reproduced with permission from [59]. e-j) Series of STM images on amorphous 2D SiO_2/Pd(1 0 0). While the sample bias is varied, certain atomic positions in the image change contrast. One 'fading wall' is presented in the zoom in the lower left corner of each scan. Scale bar 1 nm. Reproduced with permission from [23].

transition of a bubble raft [86], which again indicates that insights gained from 2D silica films can be generalized to describe other 2D amorphous systems.

To what extent the insights gained on 2D amorphous silica can be transferred to 3D amorphous solids, needs to be determined through further studies. EELS [16] and XPS [3] suggest that 2D silica is chemically equivalent to bulk silica, also pair correlation functions derived from STM data of 2D glass show good agreement to XRD and ND measurements of 3D glass, indicating structural similarities [4]. Further investigations are needed to determine the limitations of 2D SiO_2 as a model for glassy materials.

3.4. Explaining material properties through local phenomena

Thus far, we have discussed amorphous structures and local defects as an isolated topic. But investigating silica structures with high spatial resolution should ultimately lead to an improved understanding of the interrelationship of local structure and overall material properties.

SiO_2 bilayers allow studying and manipulating structures at the atomic scale with a high degree of control. By exciting the network through a focused electron beam, information on bond flipping processes was gained in a STEM study [59]. The relaxation from a cluster of two five-membered and two seven-membered rings into four hexagons is clearly visible in Fig. 16a-d. This approach reveals possible formation pathways for amorphous networks.

Observing such dynamic rearrangements on a larger scale could provide exciting new insights into the glass transition during the cooling of a melt. This thermodynamic process will be investigated in the ERC project "Crystalline and vitreous silica films and their interconversion" (2016–2020).

Working with scanning tunneling microscopy, electronic properties of 2D silica films can be addressed as well. Scanning the surface of silica bilayers on Pd(1 0 0) substrates at different sample voltages, it was found that certain atomic positions reversibly change their contrast, as shown in Fig. 16e-j [23]. These "fading walls" represent a possibility to address local vari-

Please cite this article in press as: C. Büchner, M. Heyde, Two-dimensional silica opens new perspectives, Prog. Surf. Sci (2017), https://doi.org/10.1016/j.progsurf.2017.09.001

ations in the density of states. In particular, oxygen positions involved in two seven-membered rings, or in the border of one seven-membered and one six-membered ring show this bias dependent contrast, indicating that the structural distortion influences the electronic properties. Several possible effects can be assigned for this phenomenon. The distortion might lead to re-hybridization of the involved orbitals, or the tilt in the tetrahedra may bring some atoms closer to the metal substrate than others, resulting in stronger coupling [23].

Point spectroscopy techniques that are often combined with scanning probe microscopy, might be a way to address these open questions. While scanning tunneling spectroscopy (STS) on 2D silica can be challenging due to tip instabilities, it has been used to determine the material band gap, yielding a value of 6.5 eV [48]. Comparing STS or Kelvin probe measurements from defect sites or different ring arrangements against measurements from ordered terrace sites could unlock the local electronic structure, as has been demonstrated for MgO line defects in past studies [87].

When silica bilayers are studied theoretically, an even higher degree of structural control can be exerted. Building a model *in silico* allows, in Feynman's words, to "arrange the atoms the way we want; the very *atoms*, all the way down!"[88] By introducing a well-defined amount of defects into a hexagonal sheet of silica, the influence of disorder on material properties is investigated, as well as the question: how much disorder do we need for a suitable model? A recent DFT study compared models of a hexagonal silica bilayer against a so-called haeckelite phase – a crystalline bilayer sheet formed by only five-membered and seven-membered rings [25]. Using both models, the effect of mechanical strain on the electronic properties was investigated. An MD study simplified the amorphous network by only considering ring sizes from five to eight [74].

A different approach is the stepwise introduction of 57-defects into an ordered silica sheet, while monitoring the change in properties as a function of the disorder [89]. By controlling the degree of disorder, phonon propagation in this material can be addressed, which in turn directs mechanical properties and heat conduction, both crucial parameters for technological applications. Heat transport in crystals is interpreted as phonons propagating through the bulk, which highlights that local defects and disorder must play a role in attenuating traveling waves. For the boundary case of a completely disordered glass, thermally excited hops are assumed as transport mechanism [90]. The effects of disorder are believed to play a larger role in two-dimensional materials [91]. Confinement to low dimensional specimen makes phonon propagation easier to investigate, but may also yield novel transport phenomena. In addition to heat transport, MD simulations also deliver important insights on the Young's modulus and the Poisson's ratio and how they are affected by mechanical deformation [9,92].

Theoretical studies can guide prospective experiments that corroborate electronic and mechanical properties of 2D SiO_2 films, augmenting our view of local structures directing macroscopic properties.

3.5. Benchmarks for high resolution microscopy

An atomically flat amorphous sample system is an ideal benchmarking system for advancing scanning probe microscopy (SPM). In fact, it was postulated already in 1987 that SPM is ideally suited for studying the surface of disordered structures [93]. Attempts to image surfaces of bulk oxide glasses showed that their surfaces are so corrugated that only the higher-lying fraction of the surface area could be resolved while lower areas were "hidden" [53,54,94,95]. By virtue of their atomic flatness, 2D SiO_2 films allow imaging with atomic resolution, as shown in Fig. 17 [96]. This thin film approach may also enable the study of metallic glasses in scanning probe microscopy, which suffers from the same challenges [94,97,98]. Silica bilayers are sufficiently thin for electrons to tunnel through them, which is key for employing surface science methods that rely on

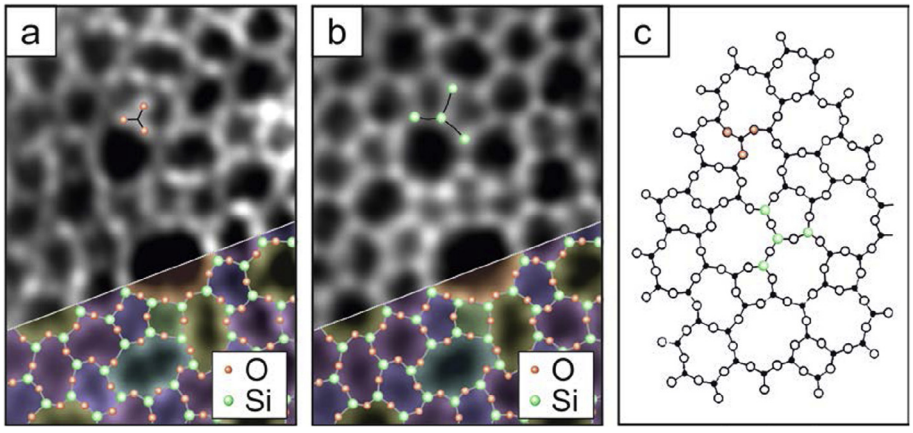

Fig. 17. Silica bilayer in atomic resolution. a) STM image of amorphous 2D silica sheet, recorded in constant height mode, showing the O positions. 2.7 nm × 3.9 nm, *Vs* = 100 mV, grey scale from 50 A (dark) to 500 pA (bright). b) AFM image recorded in parallel with a), showing the Si positions. Oscillation amplitude = 0.27 nm, grey scale from −1.0 Hz (dark) to +0.6 Hz (bright). c) Zachariasen's structure model of amorphous networks. Figure adapted with permission from [46].

Please cite this article in press as: C. Büchner, M. Heyde, Two-dimensional silica opens new perspectives, Prog. Surf. Sci (2017), https://doi.org/10.1016/j.progsurf.2017.09.001

the transport of electrons. STM or XPS measurements of thicker insulators regularly suffer from charging effects, but SiO_2 bilayers on conductive substrates do not show any such problems.

Related to the flatness of 2D silica films is the fact that their top and bottom layer of tetrahedra exhibit the same topology. This has been shown mainly by IRAS measurements which indicate the existence of Si–O–Si moieties perpendicular to the substrate, namely the bridging bonds of the bilayer [3]. The assumption that top and bottom layer consist of the same local ring arrangements is also reflected in the DFT models [3,4]. The structural identity of top and bottom plane is crucial for obtaining clear images in STEM [16], as this technique detects signals from both layers, projected on the detection plane.

The particular coordination geometry of the silica network is well suited for interpreting the observed contrast. Shown in Fig. 17a and b are two images recorded simultaneously from the same sample position in the constant height mode. The two images exhibit different atomic contrasts; a phenomenon which has been discussed for consecutive scans in STM, where it mainly correlates with changes of the microscope tip (see Fig. 5 and related discussion). However, in this case of the data shown in Fig. 17, the two imaging contrasts are observed simultaneously, recording both the tunneling and the force interaction. The contrast formation in the STM and AFM channel differ significantly, as one provides information on the local density of states the other senses the total density of state [99]. Through these conditions, as well as the unique tip termination at the time of the measurement, this complementary image contrast could be achieved.

For both images, a molecular building unit is marked with red and green spheres, respectively, in the upper part of the image. The building unit for the first image consists of three atomic positions arranged in a triangle shape, while the second image shows a windmill-shaped unit consisting of four atomic positions. The same two building blocks can be identified when considering the model for amorphous tetrahedral networks postulated by Zachariasen [67], which is shown in Fig. 17c. Comparing the model with the two STM images, structural agreement of the contrast in a) with the O positions and of the contrast in b) with the Si positions is established. Furthermore, the atomic pair distances found in both images coincide with O-O distances and Si-Si distances from XRD and ND measurements of bulk silica [46].

Fig. 17 nicely demonstrates the capabilities of a combined STM/AFM sensor, which was used to simultaneously record two images from the same sample position [100]. The tuning fork sensor carries force interaction signals and tunneling current signals without crosstalk [100], and the tip termination that was present during recording the data shown in Fig. 17 facilitated collecting complimentary information on the same surface area. The STM image in Fig. 17a shows the positions of O atoms, while Fig. 17b reveals the positions of Si atoms. The two image contrasts are observed at the same imaging parameters, as well as at other sample voltages and currents [46]. The observed contrast therefore does not directly correlate with the bias as it does in other systems, but rather is a consequence of the local tip termination. Systematic studies with chemically modified tips are needed to shed light on this variable tip contrast.

This combination of SPM techniques was also used in analyzing the contrast formation in the AFM channel in particular. Fig. 18a shows a two-dimensional mapping of the force interaction above the surface of a silica bilayer, obtained by recording constant height line scans at increasing distances from the surface [101]. The combination of all line scans forms the two-dimensional force-distance plot shown in Fig. 18a. Two positions are marked with vertical dashed lines in the plot, corresponding to positions above a pore (ring opening) and above an O atom position. At these two points, the force-distance spectra shown in Fig. 18b were extracted. Simultaneously recorded were the current-distance curves shown in Fig. 18c.

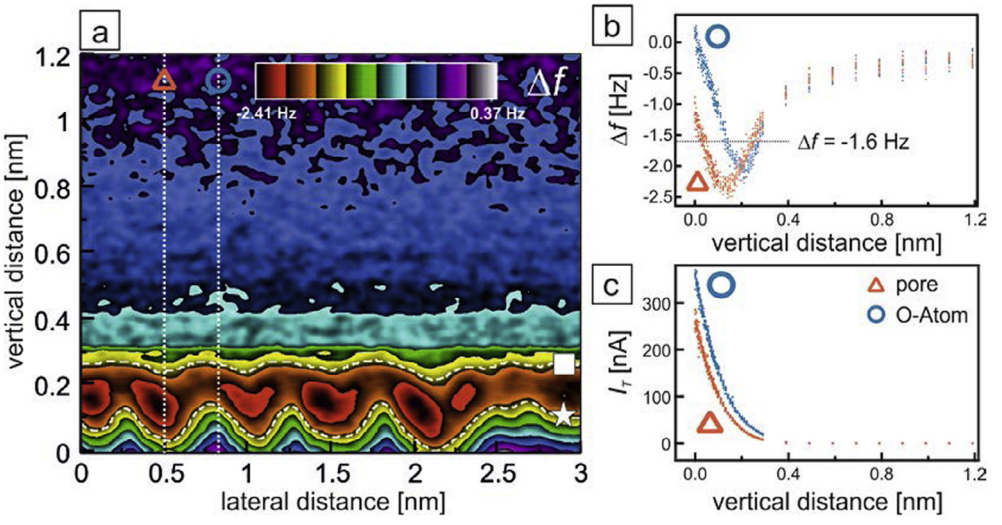

Fig. 18. a) 2D mapping of atomic force microscopy line scans recorded in constant height mode on amorphous 2D SiO_2/Ru(0 0 0 1). b) Force-distance spectra extracted from a) above an atom site and a pore site, respectively. c) Simultaneously recorded current-distance spectra. Reproduced with permission from [101].

Please cite this article in press as: C. Büchner, M. Heyde, Two-dimensional silica opens new perspectives, Prog. Surf. Sci (2017), https://doi.org/10.1016/j.progsurf.2017.09.001

While the tunneling current in c) increases monotonically with decreasing tip-surface separation, the force curves in b) show the nonmonotonic behavior that is typical for force interaction profiles. Upon approaching the surface, the force interaction first exhibits an attractive branch (positive slope), before going through a minimum and changing into the repulsive branch (negative slope). This observation simply reflects the attractive van der Waals forces acting at roughly 1 nm above the surface, and the Pauli repulsion forces increasing at very small tip-sample distances. Fig. 18b reveals that the curve on the pore is slightly shifted with respect to the position above the atom. However, the shift is measurable only in the repulsive branches. As a consequence, recording AFM images in the repulsive branch of the force interaction allows identifying atomic positions, while imaging in the attractive branch does not [101].

Studying an amorphous but atomically flat film system can be used for benchmarking high resolution microscopy techniques. Periodic features observed on a surface can be the product of tip artifacts, while well-defined amorphous structures would not. Hence, 2D SiO_2 has recently been utilized as a sample system for liquid AFM, a technique that has garnered attention for producing high resolution images of technologically relevant solid–liquid interfaces [102].

4. Chemical modifications and reactivity studies

The previous sections have considered the preparation and characterization of pure SiO_2 layers. Those systems are only the starting point, however, for a multitude of other structures that incorporate additional chemical elements and thereby increase the complexity. Several methods have been developed for chemical modification of silica bilayers during and after the initial preparation.

Doping of 2D silica layers with other cationic species can be achieved with sequential deposition or codeposition. Silicon atoms and dopant atoms are deposited on the substrate, followed by the high temperature oxidation step described in Section 2. Film preparations containing aluminum [103], iron [104] and titanium [105] have been presented, with a particular focus on structures that model the internal surfaces of zeolites. Such highly ordered, doped aluminosilicates are widely used in heterogeneous catalysis and a better understanding of their reactivity is highly desirable.

Besides incorporating elements into the bilayer film, there are also possibilities for functionalization after the film preparation. Deposition of single metal atoms on pristine silica bilayers at low temperatures has not resulted in incorporation of those atoms into the film. Rather, deposited atoms take adsorption sites either above the film or at the interface between film and substrate if penetration through the pores is feasible [50]. This observation of pristine silica bilayers being essentially unreactive against metal atoms resembles the behavior of silica monolayers [106], and is in agreement with bulk silica supports, which have to be modified prior to anchoring catalytically active groups [107,108].

A common strategy to anchor catalytically active particles to the surface of silica supports is the creation of hydroxyl groups. Furthermore, hydroxyl groups in zeolites govern their chemical behavior and are therefore a crucial ingredient to their 2D model. In order to represent these extremely important materials adequately, hydroxylation of 2D silica is a topic that is also studied intensely.

In this section, we will summarize the insights from silica doping studies and the different structures that have been obtained by introducing Al, Fe and Ti into silica bilayers. The second part of the section will deal with hydroxylation studies on silica bilayers and the chemical reactivity arising from those preparations.

These novel model systems enable new kinds of model catalysis studies, which are discussed in the last part of this section.

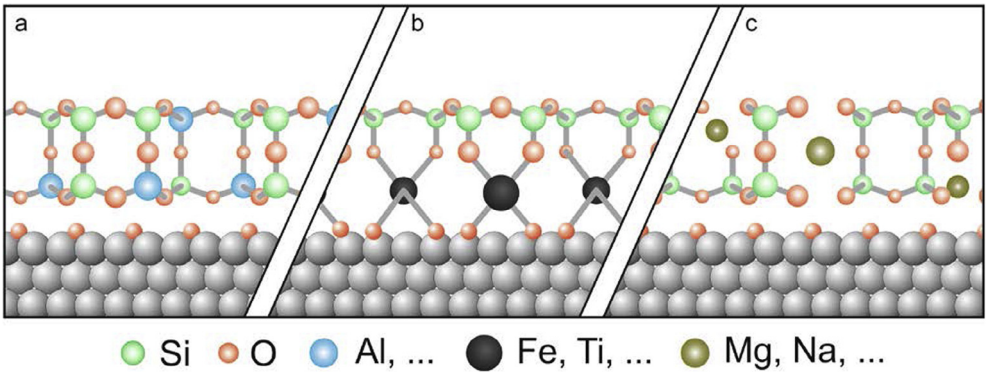

Fig. 19. Different options for incorporating cations in silica films. a) Isomorphic substitution, cations replace Si in tetrahedral building blocks. This behavior was observed for doping silica bilayers with network former aluminum. b) Formation of non-tetrahedral metal oxide building units, arranged in ordered structures underneath a silica monolayer. This behavior was observed for doping of silica thin films with the transition metals iron and titanium. c) Formation of open loop structures and coordinative disorder. This behavior is expected for doping silica thin films with network modifiers, such as magnesium.

Please cite this article in press as: C. Büchner, M. Heyde, Two-dimensional silica opens new perspectives, Prog. Surf. Sci (2017), https://doi.org/10.1016/j.progsurf.2017.09.001

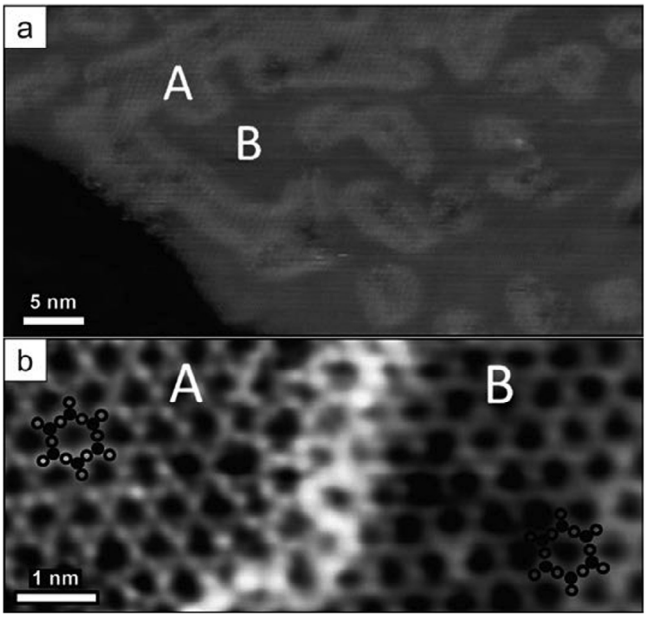

Fig. 20. STM images of a $Al_{0.12}Si_{0.88}O_2$ film. a) Large scale STM showing the segregation into two domains with distinct heights. b) Atomic resolution STM showing subtle contrast changes between domains A and B. Reproduced with permission from [103].

4.1. Metal doping in silica bilayers

There are several ways for incorporating cations into the silica bilayer, leading to distinctly different structures. Doping with Al^{3+} is an example for isomorphic substitution, where Al takes the place of Si in the tetrahedral building units, while the tetrahedral double sheet motif is preserved. Such a case is sketched in Fig. 19a. The resulting charge imbalance can be compensated by the metal substrate acting as electron reservoir or by the formation of hydroxyl groups in the vicinity of Al^{3+} sites.

Transition metals like Fe and Ti, on the other hand, cause new film structures to emerge, in which Si remains tetrahedrally coordinated, but the respective transition metal has a higher coordination number. In those structures, the transition metal polyhedra are always arranged in the bottom layer, and the silica tetrahedra in the top layer, such as shown in Fig. 19b.

A third possible case for cation incorporation is shown in Fig. 19c. This structure is expected for doping silica films with alkali or alkaline earth ions, inspired by the corresponding bulk structure models from X-ray diffraction [109]. Here, open structures with incomplete coordination polyhedra are shown. Alkali or alkaline earth metal ions are expected to take positions inside the silica pores, variably coordinated by six or more oxygen atoms.

Combining silica bilayers with other cations can contribute important insights to our understanding of solid state structures. The reduced complexity of the ultrathin film allows investigating the atomic arrangement and enables DFT calculations that would be very costly for bulk silicates. A systematic study of structural changes induced by metal dopants is therefore feasible on the 2D system. Hence, the compositional dependence of bulk glass properties, which has been studied since the invention of this material [110], can be addressed from the viewpoint of surface science.

Growth studies on incorporating small amounts of Al into the bilayer films reported the formation of segregated domains that exhibit a brighter imaging contrast in STM, as shown in Fig. 20a [103]. Both the domains containing Al (domain A) and the pure SiO_2 domains (domain B) exhibit predominantly hexagonal lattice structures, with disordered morphologies at the A-B interface (Fig. 20b). Correlating the area of domain A with the deposited fraction of aluminum implies that Al^{3+} ions preferentially substitute the tetrahedral positions in only one layer of the bilayer film. As the film preparation is carried out under ultra-high vacuum and therefore negligible amounts of water, charge compensation near Al substitution sites through hydroxyl formation is not expected. Instead, isomorphic substitution occurs preferentially in the bottom layer of the SiO_2 film, where the metal substrate can compensate charge imbalances. This preference can be corroborated with DFT calculations and is observed until the Al content of silicate films reaches 25% of the cation positions.

At higher Al contents, the terrace structures show a uniform hexagonal structure, interspersed with many local defect domains, as was shown for $Al_{0.36}Si_{0.64}O_2$ films. For Al concentrations approaching 50%, no flat, well defined films could be prepared. This observation follows Löwenstein's rule, stating that for tetrahedral coordination, no more than half of the cation sites can be filled with aluminum [111].

STM images show only the top view of the surface morphology, while IRAS characterizes the building block through their vibrational properties. The very sharp absorption band around 1300 cm^{-1} observed for SiO_2 bilayers is typically assigned to

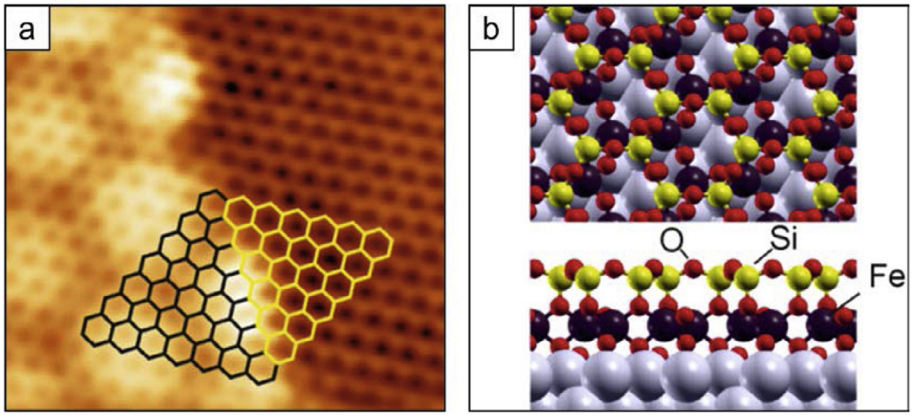

Fig. 21. Fe doped silica films. a) STM image of a Fe-containing silica domain interfacing with a pure SiO_2 domain. V_S = 1.5 V, I_T = 160 pA. b) Top view and side view of Fe-containing silica film, based on DFT calculations. Adapted with permission from [112].

the Si–O–Si groups vibrating perpendicular to the surface. Upon Al incorporation, infrared spectra show a slight red-shift of the absorption band, while the intensity and width are preserved. The observed shift suggests that some of the oscillators are modified by the isomorphic Al-substitution, but that the tetrahedral building blocks are preserved [103]. This model is supported by XPS data, showing that the overall intensity of the O1s signal is comparable across bilayer films with different Al fractions, while the intensity of a shoulder peak correlates with the amount of Al doping [103].

In contrast to Al atoms which are substituted for Si in the tetrahedral building blocks of the bilayer, adding Fe or Ti during the preparation leads to a significant change in film structure [104,105]. When Fe/Ti is deposited after the Si deposition step on a Ru(0 0 0 1) substrate, flat, well-defined films are observed in STM after the final oxidation treatment. For low Fe/Ti coverages, segregation into Fe/Ti containing (appearing higher in STM) and pure silica domains (appearing lower) is found. A region where the doped domain and the pure silicate form an interface, is shown in a high-resolution STM image in Fig. 21a. Both domains are rotated by 30° with respect to pristine SiO_2 preparations. The doped domains exhibit a clear Moiré structure, visible in STM and LEED. IR spectra of Fe-doped films show a new band at 1005 cm^{-1} (1022 cm^{-1} for Ti) in addition to the two features that characterize the pure silicate structure. The additional signal peak gains intensity as the content of the dopant is increased, while the features of silica bilayers attenuate. Based on the sharpness of the new IR signal in correlation with Fe/Ti doping, the formation of a pure FeO_2 (TiO_x respectively) layer can be excluded, since these pure oxides do not exhibit strong IR signals in this energy region. The new IRAS signal is assigned to the vibration of a Si-O-Fe/Ti moiety.

An assignment of the results to a particular film structure was made based on DFT calculations. The theoretical structure model best reproducing the change in the IR spectra is shown in Fig. 21b. Fe atoms are located on the metal in [FeO_5] square pyramids, resembling a FeO(1 1 1) phase. Above the FeO phase, a layer of [SiO_4] tetrahedra is observed. The hexagonal pores of the two layers are slightly offset. At high Fe coverages, the whole film exhibits this structure that resembles the layered structure of clay minerals [104]. A closely related structure was proposed for Ti-silicates, formed by a silica monolayer on top and a sheet of [TiO_6] octahedra between silica layer and metal substrate [105].

Preparing silicate bilayers doped with both Al and Fe showed that the transition metal atom is a strong structural driver for this system. At low Fe concentrations, the typical segregation in $Al_xSi_{1-x}O_2$ bilayer domains and Fe-silicate domains was observed. The latter structure, formed by an FeO(1 1 1)-like monolayer on the bottom and an aluminosilica monolayer on top, was the most stable structure at high Fe amounts (Fe/(Si + Al) ≈ 1) [113].

A systematic understanding of the influence of dopant atoms on the atomic structure and ring network motifs is still at the beginning. Al doped films maintain their tetrahedral bilayer structure, while incorporation of Fe/Ti leads to the formation of a pure transition metal oxide at the bottom of the film, inducing the growth of a highly ordered silica monolayer on top [112]. Growth studies with other metal dopants such as earth alkali atoms will further advance our understanding of silicate network formation. Localizing dopant atoms and identifying the surrounding structural elements requires state-of-the-art combination of microscopy and spectroscopic techniques.

4.2. Post growth hydroxylation of silica bilayers

The study of hydroxylated silica surfaces is a crucial step in bridging the materials gap for ultrathin film models. Bulk silicates typically contain dangling bonds or strained siloxane units, which readily hydroxylate when H_2O is available. For 2D silica layers prepared in ultrahigh vacuum, negligible amounts of water are typically present, and inherent hydroxyl groups are not detected. Furthermore, 2D SiO_2 films are low in defects and require significant activation in addition to excess water in order to show detectable amounts of hydroxyls. This is a chance to study the process of hydroxylation, as well as the properties of hydroxyl sites, which can be probed with high spatial resolution and discussed in context with their specific surrounding network structures.

Please cite this article in press as: C. Büchner, M. Heyde, Two-dimensional silica opens new perspectives, Prog. Surf. Sci (2017), https://doi.org/10.1016/j.progsurf.2017.09.001

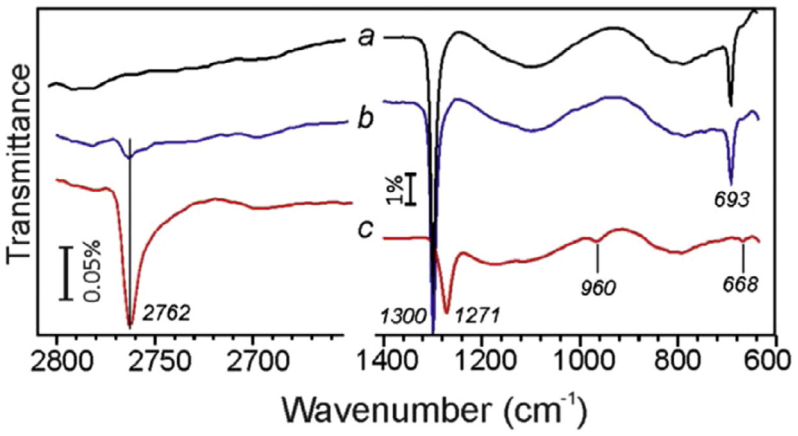

Fig. 22. IRAS curves of silica bilayers in different levels of hydroxylation with D_2O. a) "As grown" film; b) after deposition of ice layer and subsequent heating to 300 K; c) after deposition of ice layer, electron bombardment (150 eV) and subsequent heating. Reproduced with permission from [116] – Published by the PCCP Owner Societies.

Adsorption of water (D_2O is often used to discriminate against effects from residual water) on silica bilayers at room temperature does not produce hydroxyl groups that are detectable in IRAS [63]. This observation is consistent with studies on silica monolayers, which behave essentially hydrophobic [114,115]. Depositing a larger amount of water on a SiO_2/Ru (0 0 0 1) system at 100 K, and subsequently removing the ice layer by heating to 300 K did yield a new IRAS signal at 3750 cm^{-1} (2762 cm^{-1} for D_2O), indicating the formation of hydroxyl groups [63]. Fig. 22 shows an IR spectrum of the pristine silica film (black spectrum a) and after ice deposition and subsequent annealing and thermal desorption (thermal route, blue spectrum b). Detected TPD intensities of recombined water desorbing from the sample indicate a maximum hydroxyl coverage of 1.2% with respect to the Si atoms in the top layer (1 OH per 40 hexagons). Based on this low coverage, only structural defects such as step edges are believed to readily react with D_2O, while the pristine silica film is thought to be hydrophobic [63].

A higher degree of surface hydroxylation can be achieved with electron bombardment or very gentle Ar^+ bombardment of the ice layer [116]. Films prepared in this way exhibit a strong absorption band as shown in Fig. 22 (electron assisted route, red spectrum c). The IRAS intensity indicates that roughly 15% of the surface Si positions are hydroxylated, although additional groups with IR-silent vibrations might also exist [116].

This process has been investigated more closely, by hydroxylating a $Si^{18}O_2$ film using $D_2^{16}O$. After the electron bombardment, desorption of D_2O containing either ^{18}O or ^{16}O is observed in TPD, which indicates that dynamic bond-breaking and recombination occurs during the electron irradiation [117]. It has been observed that the hydroxylation yield strongly depends on the coverage of ice on the sample during irradiation, while the electron energy did not correlate as strongly with the final OD-concentration. From these findings, it is proposed that highly reactive products from water radiolysis are formed by impinging electrons, and these intermediates subsequently hydroxylate the silica bilayer [117].

Hydroxylation of Al-doped silica bilayers via the thermal route results in two new IR signals. The low-intensity $\upsilon_{O\text{-}H}$ at 3750 cm^{-1} (2763 cm^{-1} for D_2O) is the dominant vibration at low Al concentrations, analogous to hydroxylated inherent defects on pristine SiO_2. However, when more than 25% of the cationic positions are filled with Al, bridging Si-OH_{br}-Al groups can be detected at 3597 cm^{-1} (2655 cm^{-1} for D_2O) [103].

Fe silicate films showed no enhanced propensity towards hydroxylation, but in mixed Fe/Al silica bilayers, increased reactivity was observed [113]. Al-species are assumed to cause the enhanced reactivity, as their disappearance correlates with diminishing reactivity, observed for high annealing temperatures [113].

The characteristics of hydroxyl sites strongly depend on the specific silica network. Hydroxyl groups on pure SiO_2 films show only weak bonding to basic probes (CO and NH_3) [63]. Hydroxyl sites on 2D aluminosilicates on the other hand, exhibit an unusually high acidity for zeolite structures [103].

4.3. Impact of well-defined silica networks for catalysis studies

An important motivation for preparing thin silica films is the development of a suitable model system for silica-supported catalyst systems. One widely used silica-supported heterogeneous catalyst is the Phillips catalyst, polymerizing ethylene with active chromium particles [118]. This catalyst produces over one third of the annual 100 million tons of polyethylene [119]. A systematic investigation of the intermediate reaction steps and the role of the support material is therefore not merely a question of fundamental research, but resulting improvements in process efficacy would have direct environmental and economic benefits.

Monolayer $SiO_{2.5}$ films are coupled to the substrate via covalent bonds. Through this strong coupling, the metal substrate influences not only the crystal structure, but also plays a strong role in the chemical and electronic properties of the system.

Please cite this article in press as: C. Büchner, M. Heyde, Two-dimensional silica opens new perspectives, Prog. Surf. Sci (2017), https://doi.org/10.1016/j.progsurf.2017.09.001

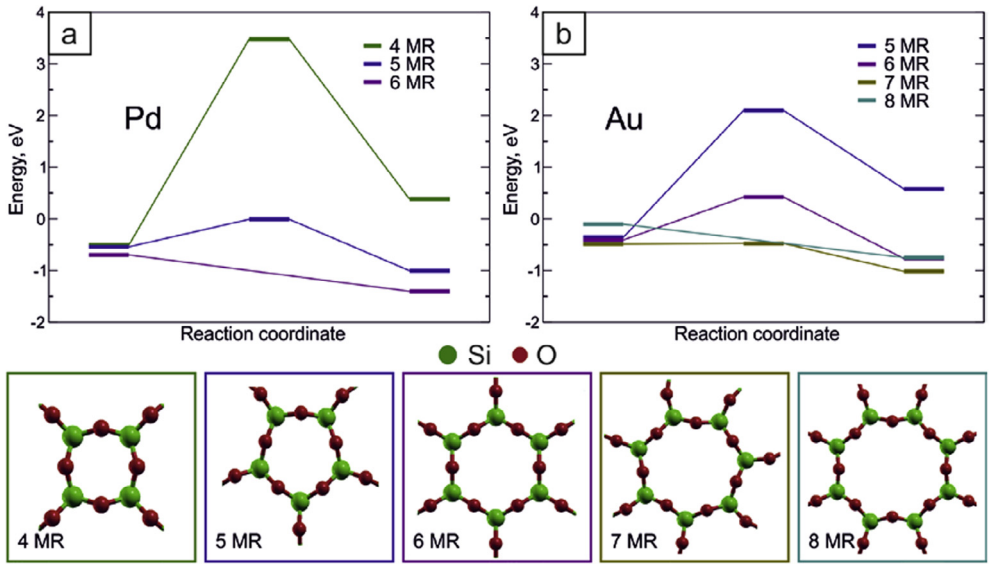

Fig. 23. Penetration barriers for Pd and Au atoms adsorbing at silica-Ru(0 0 0 1) interface. a) Energy barriers for penetration of Pd atoms through silica bilayers. b) Energy barriers for penetration of Au atoms through silica bilayers. Bottom row: models for individual silica rings used in DFT calculations. Reproduced with permission from [50].

In contrast, the bilayer film with only weak substrate-interaction is expected to be a more suitable model for silica catalyst supports. In order to build up model catalytic systems, several components need to be added to the bilayer films. A complete model would allow studying the interplay of the support material, the catalytically active species and the reactants, aiming to identify the role that each ingredient plays in the chemical reaction.

To this end, the interaction of small metal particles is investigated with the ultimate goal of anchoring catalytically active particles to the silica support. The network of silica tetrahedra in principle offers different interaction sites for metal particles, such as near an O or Si atom, or in the middle of a ring opening. The possibility to adsorb on top of, within or underneath the bilayer is an additional variable. Deposition experiments with single Au and Pd atoms showed that the preferred adsorption site is the interface between silica film and metal substrate, slightly off-center with respect to the silica rings. The different ring sizes of the silica bilayer form a size selective barrier for penetration [50]. It was found that Pd atoms adsorb on any film morphology, while Au atoms cannot penetrate the six-membered rings that form the crystalline phase. Penetration of Au atoms was observed on one type of domain boundaries (providing eight-membered rings) and on amorphous domains with ring sizes from four to eight [50]. DFT calculations (Fig. 23) investigated the energy barrier that is experienced when Au or Pd single atoms penetrate through single silica rings of different sizes (models shown in the bottom row of Fig. 23). The results show that Pd can indeed penetrate through six-membered rings, while Au needs at least the opening of an eight-membered ring to reach the interface.

DFT calculations furthermore identify that charge transfer from adsorbed atoms to the metal substrate contributes substantially to the stabilization of the adsorbates at the interface. This is found when comparing the interaction of Na or Mg atoms with a free-standing vs. a supported silica bilayer [52]. The global energy minimum position is adsorption at the interface, although energy barriers for penetrating the film can be significant.

At this point, no case has been found for adsorbing small species inside the bilayer, where they would be coordinated on all sides by a silica-cage. This would be an interesting model for studying the metal species interacting predominantly with the oxide support. However, it is generally assumed that when the ring size allows penetration, the global minimum position at the interface is also accessible. Another promising option would be to study metals on top of the film, which are too large for penetrating the pores. This might be done with single atoms or with small clusters on top of the silica bilayer. In the case of silica monolayers, Pd atoms adsorbed at the interface have been used as anchoring points for metal clusters [120].

While the pristine silica bilayer is inert, the introduction of dopants like Al into the network induces electronic states, leading to stronger interactions with small species [52]. A DFT study found that Al-doped silica films interact strongly with Na atoms, which adsorb on the surface of the bilayer, not inside the silica cage. Generally, cation doping can enhance the chemical activity of silicates, so the same is not surprising for silica bilayers [121].

In order to understand the chemical reactivity of this model system, the interaction of small molecules with the structurally complex network of silica bilayer films must be characterized as well.

During the growth of this system, the interaction of O_2 molecules with the SiO_2/Ru(0 0 0 1) can be studied. Underneath the 2D SiO_2 film, the Ru(0 0 0 1) substrate can exist with different oxygen coverages. These can be changed reversibly by heating the sample in UHV, H_2 or in O_2, respectively, without affecting the film structure itself [30,122]. Hence, O_2 molecules are clearly able to penetrate the film structure, and dissociate at the metal. It is interesting to note that the presence of the

silica film limits the amount of adsorbed oxygen at the interface, so that the formation of a RuO_2 passivation layer is prevented [123]. It was also observed that the respective uptake of CO and D_2 on the Ru(0 0 0 1) is lowered by 35% by the presence of a SiO_2 bilayer. This effect is enhanced in the case of aluminosilicate films, which are more strongly coupled to the substrate and only allow oxygen coverages below 0.5 [122].

The passivating effect of the silica film is reflected not only in decreased gas uptake, but also in the temperature dependence that is observed for gas penetration. Temperature dependent absorption experiments showed that below 200 K, CO absorption is severely hindered [124]. This effect is assigned to CO adsorbates blocking the large ring openings, which are the only feasible adsorption sites. At temperatures above 200 K, the adsorbed CO molecules become more mobile, and thus are able to vacate the adsorption pathways. A similar site blocking effect was observed for pre-adsorption of CO, which subsequently lowered the D_2 uptake [124].

In the gas adsorption experiments described thus far, no chemical interaction of the gas molecules and the pristine SiO_2 film was detected. Conversely, hydroxyls on 2D SiO_2 films represent inherently active sites on an inert, structurally well-defined substrate. They are suitable for anchoring reactant molecules on the surface, which can then be probed with high spatial and chemical precision through state-of-the-art surface science tools. Especially changes in the vibrational properties of OH(OD)-groups can be measured to infer their reactivity.

The hydroxyl groups obtained on 2D SiO_2 via thermal hydroxylation films show a high degree of stability, and even for high CO exposures no alteration in the IRAS signals was observed [63]. Adsorption of NH_3 molecules caused attenuation of the hydroxyl vibration in infrared spectra, indicating the abstraction of the proton by the strong base. Upon desorption, the hydroxyl groups are recovered on the silica film. Through isotopic labeling and combined IRAS and TPS studies, hydrogen-scrambling between OD-groups and NH_3 was revealed [63].

In comparison to SiO_2 films, the hydroxylated Al-doped SiO_2 films on Ru(0 0 0 1) showed more reactive hydroxyl groups, as evidenced by altered IRAS absorption features. In particular, changes in the absorption feature linked to bridging Si-OH_{br}-Al, which are unique to films with more than 25% Al content, imply strong interaction with the studied probe molecules. Upon CO-adsorption, OH(OD)-groups on $Al_xSi_{1-x}O_2$ bilayer films show a red-shift of 379 cm^{-1} (243 cm^{-1} for OD), which is much larger than values observed for the acidic sites in 3D zeolites [103]. Correspondingly, a strong red-shift of 487 cm^{-1} (394 cm^{-1} for OD) was observed in case of adsorbing the weak base C_2H_4 on hydroxylated films [125]. The ethene-silica adduct formed via the hydroxyl group deserves particular attention, as it represents a likely intermediate in the polymerization reaction of ethene.

In contrast to weak bases, the adsorption of strong bases like pyridine or ammonia leads to an abstraction of the proton, detected as the disappearance of the hydroxyl vibration band in IRAS [125]. It is assumed that such simple molecules on the hydroxylated silica film can be studied individually to learn about the interplay of each functional group with the surface, which allows inferring the interaction of more complex organic molecules with inorganic surfaces [126].

As the 2D silica system is uniquely accessible to many surface science techniques, further insights can surely be gained by studying the chemical properties of silica bilayers with high spatial resolution. Specifically, state of the art-microscopy could identify preferred hydroxylation sites and provide a correlation between reactivity of hydroxyl groups and their surrounding network structure.

Besides modeling industrial heterogeneous catalysts, metal supported silica bilayers represent an opportunity to study reactions in confined space. This research field considers how small and well defined environments can be used to tailor the reactive properties of a chemical system [127]. Those nanocavities can be created in many ways, such as porous oxides, supramolecular cages or by addressing the interface space between 2D materials and their support. Species that are trapped at the interface can exhibit modified reactivities due to confinement effects and a stronger influence of local defects [128].

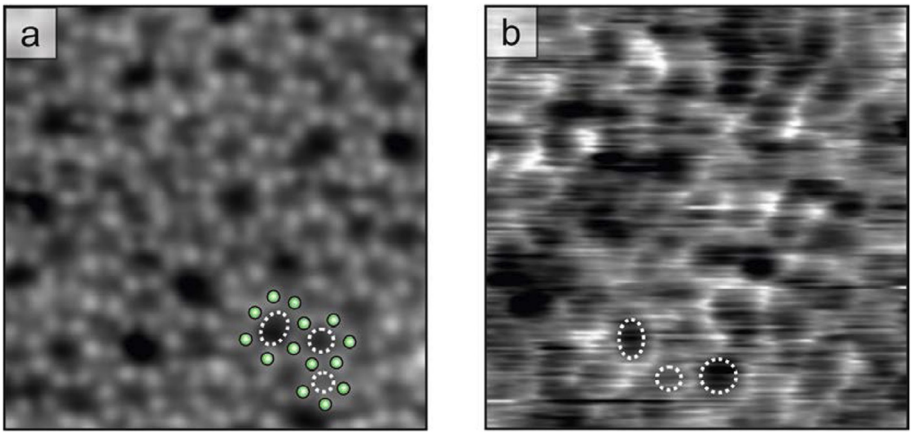

Fig. 24. a) Atomic resolution STM image of silica bilayer in UHV. Some of the Si positions are marked with green spheres. The respective rings are marked with white dashed ellipses. b) Ring resolution AFM image of a silica bilayer in liquid. Some rings are marked with white dashed ellipses. Reproduced with permission from [102]. (For interpretation of the references to color in this figure legend, the reader is referred to the web version of this article.)

Please cite this article in press as: C. Büchner, M. Heyde, Two-dimensional silica opens new perspectives, Prog. Surf. Sci (2017), https://doi.org/10.1016/j.progsurf.2017.09.001

The silica bilayer system offers different ways to influence "reactions under cover". It has been shown that intercalating varying amounts of oxygen to the substrate-film interface will change the work function [50]. An in-depth investigation of the changes to the electronic structure at the interface is promising for controlling reactivity [51]. Adsorbates such as O_2 or CO change the interface spacing, essentially "pushing" the film away from the substrate at high adsorbate coverages [30,124,129], providing a way to tune the confined space.

5. Silica bilayers as 2D materials

Up to this point, we have considered 2D silica films as useful model systems, allowing us to study structures, defects, glass properties and catalysis under well-defined conditions with reduced complexity. It is worthwhile, however, to explore silica bilayers as independent 2D materials. In particular, 2D SiO_2 may be useful as an ultrathin electrical insulator on the one hand, and as a highly permselective membrane on the other hand.

Silica bilayers show a degree of chemical stability that is not necessarily expected for ultrathin films, which is promising for handling and incorporating them into devices. The double sheet structure with fully saturated valences withstands deterioration even under month-long exposure to air and ambient humidity [16]. Liquid-AFM images show that the structure is retained at the nanoscale, during prolonged imaging in water and NaCl solutions [102]. Fig. 24a presents the atomically resolved STM of an amorphous silica bilayer, recorded in UHV at low temperature. The imaging contrast reveals the Si atoms arranged in the typical fashion of an amorphous silica bilayer. An equivalent sample was removed from the vacuum chamber and imaged at room temperature, while submerged in a 400 mM aqueous NaCl solution. In the liquid-AFM image shown in Fig. 24b, the network of different ring sizes can be identified, and their spatial arrangement concurs with the typical networks observed in UHV-based STM images [102]. It is important to note that decomposition of 2D silica has been observed in acidic and alkaline conditions, providing a quantitative link from the model system to analogous bulk systems [117,121].

The self-saturated bilayer structure exhibits no covalent bonds between the film and its substrate. Only weak interaction binds the 2D SiO_2 film to the metal surface, but this adhesion can be further decreased by intercalating O_2 or CO molecules [30,124]. Due to this weak interaction, it is possible to exfoliate the silica film and transfer it to another support material.

This was demonstrated recently using a polymer-assisted transfer protocol [36]. The silica bilayer is initially grown on a Ru(0 0 0 1) substrate. LEED indicates a predominantly amorphous silica bilayer, and the STM images (see Fig. 25a) reveal a coverage of 1.6 ML. This sample can be removed from the UHV chamber, and covered with a thin film of poly(methyl methacrylate) (PMMA) by spin coating. By mechanically exfoliating the polymer film, the silica film is lifted off the substrate and supported on the polymer.

After this step, the plain Ru(0 0 0 1) growth substrate can be transferred back into a vacuum chamber to verify the successful exfoliation. Fig. 25b shows the STM image of the plain metal surface, and LEED and AES data verify the complete removal of the SiO_2 layer by the mechanical exfoliation step [36].

A plain Pt(1 1 1) crystal was used as new substrate. Fig. 25c shows the typical flat terraces of the metal substrate before the film transfer. The PMMA film supporting the silica bilayer is placed on the new substrate, and the polymer is removed by applying a gentle heating step. Subsequently, the sample is investigated with STM (shown in Fig. 25d), LEED and AES, confirming the successful transfer of the 2D SiO_2 layer. The STM data give a coverage value of 1.6 ML, indicating that the transfer did not lead to material losses. This assumption was verified using environmental scanning electron microscopy (ESEM), showing that the whole crystal surface ($\sim$1 cm^2) was covered by the transferred film [36].

This proof of principle makes 2D silica accessible for device building and allows to fully explore its performance potential in various applications. However, the presented method was successful for transferring only a certain type of silica bilayer. In Fig. 3, a complex parameter space of substrate choice, surface coverage and other preparation parameters was indicated. The

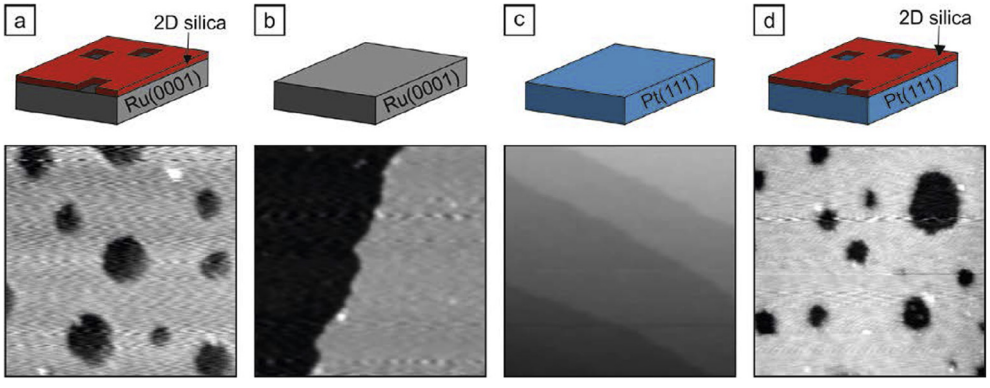

Fig. 25. a-d) STM images of different stages of a 2D silica transfer, all scans 50 × 50 nm. a) As-grown silica film on Ru(0 0 0 1), V_S = 1 V, I_T = 50 pA. b) Plain Ru (0 0 0 1) after exfoliation of a silica film, V_S = 2 V, I_T = 50 pA. c) Plain Pt(1 1 1) substrate before transfer of a silica film, V_S = 0.5 V, I_T = 50 pA. d) Transferred silica film on Pt(1 1 1), V_S = 1 V, I_T = 100 pA.

Please cite this article in press as: C. Büchner, M. Heyde, Two-dimensional silica opens new perspectives, Prog. Surf. Sci (2017), https://doi.org/10.1016/j.progsurf.2017.09.001

resulting silica bilayer films exhibit varying amounts of crystalline vs. amorphous regions, of mesoscopic holes, and differences in film-substrate interaction. The transfer study reported in [36] investigated 2D SiO_2 films grown with different procedures, but always supported on Ru(0 0 0 1). Films with a surface coverage from 1.5 ML to 1.8 ML, which are predominantly amorphous, were exfoliated successfully. Bilayers with a higher surface coverage were unaffected by the PMMA-assisted exfoliation step. There are different possible explanations for this observation. In the films with lower coverage, the relief of mesoscopic holes might provide more points of static friction for the PMMA layer. Alternatively, as high-coverage films typically show more crystalline silica domains in registry with the substrate, providing more contact points for efficient van der Waals interaction might be the underlying reason for the stronger film-substrate adhesion. In general, silica bilayers are expected to interact with the substrate only via van der Waals forces. Hence, most silica bilayer films will likely be transferrable with slight modifications in the exfoliation procedure. Completely amorphous films [11], films without substrate registry [13], or systems where adsorbed molecules decrease the substrate interaction [129] are especially promising candidates for further transfer experiments.

Furthermore, in analogy to the 2D material graphene, scalability is a challenge that must be solved before real world applications can be realistically implemented [35]. Efforts of scaling up should focus both on large scale growth, and automated exfoliation techniques to produce high quality SiO_2 bilayers efficiently.

The sieve-like property of 2D SiO_2 which was demonstrated by size selective penetration of metals and molecules may be exploited in filtration. Areas like gas separation or water purification could benefit from the bilayer membrane that exhibits well-defined pore diameters (providing selectivity) and is ultrathin (optimizing permeation). To this end, a freestanding silica membrane needs to be provided, which is accessible for a filtrate to pass through from one side to the other. Transferring the 2D sheet onto a grid or holey support could yield such a freestanding silica bilayer. Conversely, the blockage of molecules by the silica film can be employed as anticorrosion coating. A prerequisite is the development of a procedure for coating the sensitive surface with a hole-free silica film.

Several properties of 2D silica films recommend them as promising materials for building 2D heterostructures. One of them is the atomic flatness of silica layers. Thermally grown sub-nm silica layers on Si wafers have been studied intensely, to produce silica supports for 2D materials. However, progress in this field has been hampered by an ill-defined Si/SiOx interface and resulting silica structures that can be unordered and rough [130–132]. This roughness is problematic for supported graphene layers, as the induced deformation severely decreases the conductivity [133]. Currently, van der Waals heterostructures frequently employ hexagonal boron nitride layers as insulating component, but 2D silica may present a useful alternative.

A transfer-free approach for producing van der Waals heterostacks might be the direct preparation of 2D SiO_2 under or on top of other 2D materials. Such a stack of a silica bilayer grown under graphene has been observed, possibly proceeding via solid state growth [16]. In a different study, physical vapor deposition of Si was used to intercalate Si at a Gr/Ir(1 1 1) interface. The Si layer was subsequently oxidized to a ~1.6 nm thick SiO_2 film [134]. Therefore, a direct growth by intercalation is feasible. The opposite approach, intercalating another material to the SiO_2/support interface, might also be possible. In comparison to graphene, the ring openings or pores in a silica film are on average twice as large. Adsorption experiments with single Au and Pd atoms, and with small molecules have revealed a size-selective penetration of the silica film [50,124], which can be exploited to grow silica layers in a van der Waals stack.

A key aspect of employing 2D silica films in nanoelectronic devices is their insulating nature. Their bulk counterparts are known for their exceptionally large band gaps. The band structure of silica bilayers has been investigated by various groups using DFT calculations [16,25,50], reporting values of up to 7.3 eV, depending on the atomic structure. Biaxial strain of around 15% can reduce the band gap to about 2 eV as shown in Fig. 26, while uniaxial strain beyond 30% could achieve band gaps smaller than 1 eV [25]. This extremely wide range of strain-induced band gaps indicates a potential use of silica bilayers

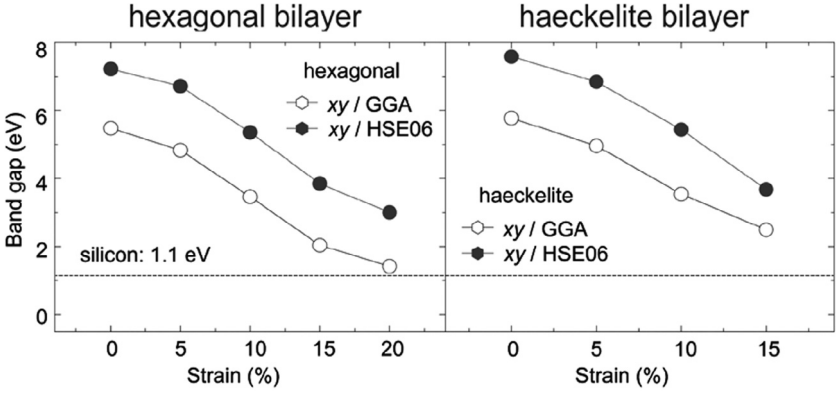

Fig. 26. Plot of a hexagonal silica bilayer band gap vs. strain and a haeckelite bilayer (crystalline arrangement of five- and seven-membered rings) band gap vs. strain. Reproduced with permission from [25].

Please cite this article in press as: C. Büchner, M. Heyde, Two-dimensional silica opens new perspectives, Prog. Surf. Sci (2017), https://doi.org/10.1016/j.progsurf.2017.09.001

Table 2
Experimentally measured direct band gaps for different 2D materials.

2D Material	Band gap	Measured by	Reference
Graphene	0 eV	electronic transport	[135]
$MoSe_2$	1.55 eV	optical spectroscopy	[136]
MoS_2	1.9 eV	optical spectroscopy	[137]
Black phosphorous	2 eV	STS	[138]
h-BN	5.56 eV	UV–vis absorption	[139]
2D SiO_2	6.5 eV	STS	[48]

in sensor applications. Scanning tunneling spectroscopy measurements corroborate a band gap of 6.5 eV [48], which is larger than that of any other 2D material at this point. See Table 2 for an overview of experimentally measured band gaps for commonly studied 2D materials. Hence, 2D SiO_2 represents a viable option for insulating layers in nanoelectronic devices. An early study demonstrated the possibility to grow well-defined silica bilayers under graphene in a flat stack [16], but did not comment on the electronic properties of the supported graphene.

EELS measurements detecting the Si conduction band-induced gap states extending through a SiO_2 gate layer concluded that an effective tunneling barrier needs to be 0.7–1.2 nm thick to suppress the electronic spillover [130]. This requirement would be met by stacking two silica bilayers, which are extremely flat and low in defects, thereby providing a low-loss environment for semiconductors and conductors. Further studies are needed regarding stacking several silica bilayers, either during growth or by transferring several bilayer films to the same support.

6. Conclusion

2D silica is promising as material for technological applications, but also as a model system for studying fundamental physical phenomena. [SiO_4] tetrahedral building blocks arrange in a coordinatively saturated bilayer, forming a nanosheet with a surface flatness corresponding to the single crystal substrate. Through choosing appropriate preparation parameters, films can be driven towards crystalline or amorphous topologies, while also exhibiting mesoscopic holes.

The reliable preparation of self-saturated bilayer films with high structural control is the starting point for several distinct lines of research. Several growth studies for 2D silica films have been reported in the last years, and structural, electronic, vibrational and chemical properties of silica films are now in the focus. Studying defect features at the atomic level in this technologically important material allows drawing conclusions about their impact on structural properties. Analyzing extended disordered regions advances our understanding about amorphous materials, which have so far not been directly accessible with real space atomic resolution. Precise control over the local structure has the potential to shed light on many structure–property relationships, such as heat transport. The non-periodic systems with extremely low surface corrugation can also serve as benchmarking system for microscopy techniques.

Applying silica bilayer structures in model catalysis enables precise monitoring of all chemical changes throughout functionalization and subsequent reaction. 2D silica-supported model catalysts are expected to advance our understanding of metal-nanoparticles interacting with supports and with reactants, as the structural simplification provided by 2D silica in comparison with 3D silica is key for developing highly accurate theoretical models, which in turn allow unequivocal assignments of experimental data. Furthermore, the confined space between pristine 2D silica films and their substrate provides the option to study reactions in nano-volumes.

Through recent exfoliation and transfer studies, 2D silica films have been made accessible for nanoelectronic device assembling and other 2D material applications. Their durability and large band gap renders them a useful addition to the library of 2D materials. Application in heterostacks and other nanodevices will require further insights in transferring, handling and manipulating 2D silica films, ideally with scaleable methods. Stacking several bilayers would allow precise control over insulator thickness.

Based on the pure SiO_2 bilayer preparation, a vast array of related structures has either been prepared or hypothesized. In this review, we have briefly touched upon doped bilayers, surface functionalization and their resulting chemical reactivity, but it is assumed that the field of chemically modified silica bilayers will warrant its own review paper in the future.

Acknowledgement

The authors would like to thank Joachim Sauer (Humboldt Universität zu Berlin) and Gianfranco Pacchioni (Università degli Studi di Milano-Bicocca) for invaluable discussions throughout our collaborations. Most importantly, this article would have been impossible without the support of Hans-Joachim Freund, as well as many of the colleagues in the Department for Chemical Physics whose work has been cited.

We gratefully acknowledge the Collaborative Research Center SFB 1109 for financial support.

Please cite this article in press as: C. Büchner, M. Heyde, Two-dimensional silica opens new perspectives, Prog. Surf. Sci (2017), https://doi.org/10.1016/j.progsurf.2017.09.001

References

[1] S. Shaikhutdinov, H.-J. Freund, Ultrathin silica films on metals: the long and winding road to understanding the atomic structure, Adv. Mater. 25 (2013) 49–67, https://doi.org/10.1002/adma.201203426.
[2] T. Schroeder, M. Adelt, B. Richter, M. Naschitzki, M. Bäumer, H.-J. Freund, EPITAXIAL GROWTH OF SiO 2 ON Mo(112), Surf. Rev. Lett. 7 (2000) 7–14, https://doi.org/10.1142/S0218625X00000038.
[3] D. Löffler, J.J. Uhlrich, M. Baron, B. Yang, X. Yu, L. Lichtenstein, et al, Growth and structure of crystalline silica sheet on, Phys. Rev.Lett. 105 (2010) 146104, https://doi.org/10.1103/PhysRevLett. 105.146104.
[4] L. Lichtenstein, C. Büchner, B. Yang, S.K. Shaikhutdinov, M. Heyde, M. Sierka, The atomic structure of a metal-supported vitreous thin silica film, Angew. Chemie, Int. Ed. 51 (2012) 404–407, https://doi.org/10.1002/anie.201107097.
[5] J.-B. Michel, Y.K. Shen, A.P. Aiden, A. Veres, M.K. Gray, J.P. Pickett, et al, Quantitative analysis of culture using millions of digitized books, Science 80 (331) (2011) 176–182, https://doi.org/10.1126/science.1199644.
[6] A. Weiss, A. Weiss, Über Siliciumchalkogenide. VI. Zur Kenntnis der faserigen Siliciumdioxyd-Modifikation, Zeitschrift Für Anorg. Und Allg, Chemie. 276 (1954) 95–112, https://doi.org/10.1002/zaac.19542760110.
[7] S.K. Shaikhutdinov, H.-J. Freund, Ultra-thin silicate films on metals, J. Phys. Condens. Matter. 27 (2015) 443001, https://doi.org/10.1088/0953-8984/27/44/443001.
[8] V.O. Özçelik, S. Cahangirov, S. Ciraci, Stable Single-Layer Honeycomblike Structure of Silica, Phys. Rev. Lett. 112 (2014) 246803, https://doi.org/10.1103/PhysRevLett. 112.246803.
[9] Z. Gao, X. Dong, N. Li, J. Ren, Novel Two-Dimensional Silicon Dioxide with in-Plane Negative Poisson's Ratio, Nano Lett. 17 (2017) 772–777, https://doi.org/10.1021/acs.nanolett.6b03921.
[10] G. Wang, G.C. Loh, R. Pandey, S.P. Karna, Novel Two-Dimensional Silica Monolayers with Tetrahedral and Octahedral Configurations, J. Phys. Chem. C 119 (2015) 15654–15660, https://doi.org/10.1021/acs.jpcc.5b01646.
[11] X. Yu, B. Yang, J.A. Boscoboinik, S.K. Shaikhutdinov, H.-J. Freund, Support effects on the atomic structure of ultrathin silica films on metals, Appl. Phys. Lett. 100 (2012) 151608, https://doi.org/10.1063/1.3703609.
[12] E.I. Altman, J. Götzen, N. Samudrala, U.D. Schwarz, Growth and Characterization of Crystalline Silica Films on Pd(100), J. Phys. Chem. C 117 (2013) 26144–26155, https://doi.org/10.1021/jp4101152.
[13] J.-H. Jhang, C. Zhou, O.E. Dagdeviren, G.S. Hutchings, U.D. Schwarz, E.I. Altman, Growth of two dimensional silica and aluminosilicate bilayers on Pd (111): from incommensurate to commensurate crystalline, Phys. Chem. Chem. Phys. (2017), https://doi.org/10.1039/C7CP02382K.
[14] G.S. Hutchings, J.-H. Jhang, C. Zhou, D. Hynek, U.D. Schwarz, E.I. Altman, Epitaxial Ni x Pd 1– x (111) Alloy Substrates with Continuously Tunable Lattice Constants for 2D Materials Growth, ACS Appl. Mater. Interfaces. 9 (2017) 11266–11271, https://doi.org/10.1021/acsami.7b01369.
[15] F. Ben Romdhane, T. Björkman, J.A. Rodríguez-Manzo, O. Cretu, A.V. Krasheninnikov, F. Banhart, In Situ Growth of Cellular Two-Dimensional Silicon Oxide on Metal Substrates, ACS Nano 7 (2013) 5175–5180, https://doi.org/10.1021/nn400905k.
[16] P.Y. Huang, S. Kurasch, A. Srivastava, V. Skakalova, J. Kotakoski, A.V. Krasheninnikov, et al, Direct Imaging of a Two-Dimensional Silica Glass on Graphene, Nano Lett. 12 (2012) 1081–1086, https://doi.org/10.1021/nl204423x.
[17] X. Xu, D.W. Goodman, New approach to the preparation of ultrathin silicon dioxide films at low temperatures, Appl. Phys. Lett. 61 (1992) 774–776, https://doi.org/10.1063/1.107795.
[18] J.-W. He, X. Xu, J.S. Corneille, D.W. Goodman, X-ray photoelectron spectroscopic characterization of ultra-thin silicon oxide films on a Mo(100) surface, Surf. Sci. 279 (1992) 119–126, https://doi.org/10.1016/0039-6028(92)90748-U.
[19] X. Xu, D.W. Goodman, The preparation and characterization of ultra-thin silicon dioxide films on a Mo(110) surface, Surf. Sci. 282 (1993) 323–332, https://doi.org/10.1016/0039-6028(93)90937-F.
[20] J. Weissenrieder, S. Kaya, J.-L. Lu, H.-J. Gao, S. Shaikhutdinov, H.-J. Freund, et al, Atomic structure of a thin silica film on a Mo(112) substrate: a two-dimensional network of SiO_4 tetrahedra, Phys. Rev. Lett. 95 (2005) 76103, https://doi.org/10.1103/PhysRevLett. 95.076103.
[21] B. Yang, W.E. Kaden, X. Yu, J.A. Boscoboinik, Y. Martynova, L. Lichtenstein, et al, Thin silica films on Ru(0001): monolayer, bilayer and three-dimensional networks of [SiO4] tetrahedra, Phys. Chem. Chem. Phys. 14 (2012) 11344, https://doi.org/10.1039/c2cp41355h.
[22] H.W. Klemm, G. Peschel, E. Madej, A. Fuhrich, M. Timm, D. Menzel, et al, Preparation of silica films on Ru(0001): a LEEM/PEEM study, Surf. Sci. 643 (2016) 45–51, https://doi.org/10.1016/j.susc.2015.05.017.
[23] E.I. Altman, U.D. Schwarz, Structural and Electronic Heterogeneity of Two Dimensional Amorphous Silica Layers, Adv. Mater. Interfaces. 1 (1400108) (2014) 1–5, https://doi.org/10.1002/admi.201400108.
[24] L. Lichtenstein, M. Heyde, H.-J. Freund, Crystalline-Vitreous Interface in Two Dimensional Silica, Phys. Rev. Lett. 109 (106101) (2012) 1–5, https://doi.org/10.1103/PhysRevLett. 109.106101.
[25] E. Gao, B. Xie, Z. Xu, Two-dimensional silica: structural, mechanical properties, and strain-induced band gap tuning, J. Appl. Phys. 119 (2016) 14301, https://doi.org/10.1063/1.4939279.
[26] A. Malashevich, S. Ismail-Beigi, E.I. Altman, Directing the Structure of Two-Dimensional Silica and Silicates, J. Phys. Chem. C 120 (2016) 26770–26781, https://doi.org/10.1021/acs.jpcc.6b07008.
[27] L. Lichtenstein, The Structure of Two-Dimensional Vitreous Silica, Freie Universität Berlin, 2012.
[28] F. Ben Romdhane, T. Björkman, A.V. Krasheninnikov, F. Banhart, Solid-State Growth of One- and Two-Dimensional Silica Structures on Metal Surfaces, J. Phys. Chem. C 118 (2014) 21001–21005, https://doi.org/10.1021/jp506114k.
[29] S. Pomp, W.E. Kaden, M. Sterrer, H.-J. Freund, Exploring Pd adsorption, diffusion, permeation, and nucleation on bilayer SiO2/Ru as a function of hydroxylation and precursor environment: from UHV to catalyst preparation, Surf. Sci. 652 (2016) 286–293, https://doi.org/10.1016/j.susc.2015.12.030.
[30] R. Włodarczyk, M. Sierka, J. Sauer, D. Löffler, J.J. Uhlrich, X. Yu, et al, Tuning the electronic structure of ultrathin crystalline silica films on Ru(0001), Phys. Rev. B. 85 (2012) 85403, https://doi.org/10.1103/PhysRevB.85.085403.
[31] S.F. Swallen, K.L. Kearns, M.K. Mapes, Y.S. Kim, R.J. McMahon, M.D. Ediger, et al, Organic glasses with exceptional thermodynamic and kinetic stability, Science 80 (315) (2007) 353–356, https://doi.org/10.1126/science.1135795.
[32] D. Turnbull, Metastable structures in metallurgy, Metall. Trans. A 12 (1981) 695–708, https://doi.org/10.1007/BF02648333.
[33] E.D. Zanotto, Do cathedral glasses flow?, Am J. Phys. 66 (1998) 392–395, https://doi.org/10.1119/1.19026.
[34] I.S. Gutzow, J.W.P. Schmelzer, The Vitreous State, Springer, Berlin Heidelberg, Berlin, Heidelberg (2013), https://doi.org/10.1007/978-3-642-34633-0.
[35] A.C. Ferrari, F. Bonaccorso, V. Falko, K.S. Novoselov, S. Roche, P. Bøggild, et al, Science and technology roadmap for graphene, related two-dimensional crystals, and hybrid systems, Nanoscale. 7 (2015) 4598–4810, https://doi.org/10.1039/C4NR01600A.
[36] C. Büchner, Z.-J. Wang, K.M. Burson, M.-G. Willinger, M. Heyde, R. Schlögl, et al, A Large-Area Transferable Wide Band Gap 2D Silicon Dioxide Layer, ACS Nano 10 (2016) 7982–7989, https://doi.org/10.1021/acsnano.6b03929.
[37] M. Choi, K. Na, J. Kim, Y. Sakamoto, O. Terasaki, R. Ryoo, Stable single-unit-cell nanosheets of zeolite MFI as active and long-lived catalysts, Nature 461 (2009) 246–249, https://doi.org/10.1038/nature08288.
[38] A.M. Doyle, G. Rupprechter, N. Pfänder, R. Schlögl, C.E.A. Kirschhock, J.A. Martens, et al, Ultra-thin zeolite films prepared by spin-coating Silicalite-1 precursor solutions, Chem. Phys. Lett. 382 (2003) 404–409, https://doi.org/10.1016/j.cplett.2003.10.088.
[39] X. Wang, J. Xu, Q. Wang, A. Xu, Y. Zhai, J. Luo, et al, Wet Chemical Synthesis of Silica Nanosheets via Ethyl Acetate-Mediated Hydrolysis of Silica Precursors and Their Applications, Small 13 (2017) 1603369, https://doi.org/10.1002/smll.201603369.
[40] C. Braun, H. Ehrenberg, W. Schnick, $BaSi_4O_6N_2$ – a hexacelsian-type layered oxonitridosilicate, Eur. J. Inorg. Chem. 2012 (2012) 3923–3928, https://doi.org/10.1002/ejic.201200186.

Please cite this article in press as: C. Büchner, M. Heyde, Two-dimensional silica opens new perspectives, Prog. Surf. Sci (2017), https://doi.org/10.1016/j.progsurf.2017.09.001

[41] A. Corma, V. Fornes, S.B. Pergher, T.L.M. Maesen, J.G. Buglass, Delaminated zeolite precursors as selective acidic catalysts, Nature 396 (1998) 353–356, https://doi.org/10.1038/24592.
[42] F. Liebau, Structural Chemistry of Silicates, Springer, Berlin Heidelberg, Berlin, Heidelberg (1985), https://doi.org/10.1007/978-3-642-50076-3.
[43] H. Hwang, D. Seoung, G.D. Gatta, D.A. Blom, T. Vogt, Y. Lee, Topotactic and reconstructive changes at high pressures and temperatures from Cs-natrolite to Cs-hexacelsian, Am. Mineral. 100 (2015) 1562–1567, https://doi.org/10.2138/am-2015-5090.
[44] M. Jałochowski, K. Palotás, M. Krawiec, Spilling of electronic states in Pb quantum wells, Phys. Rev. B. 93 (2016) 35437, https://doi.org/10.1103/PhysRevB.93.035437.
[45] K. Højrup Hansen, T. Worren, E. Lægsgaard, F. Besenbacher, I. Stensgaard, Bias dependent apparent height of an Al2O3 thin film on NiAl(110), and of supported Pd clusters, Surf. Sci. 475 (2001) 96–102, https://doi.org/10.1016/S0039-6028(00)01077-3.
[46] L. Lichtenstein, M. Heyde, H.-J. Freund, Atomic arrangement in two-dimensional silica: from crystalline to vitreous structures, J. Phys. Chem. C 116 (2012) 20426–20432, https://doi.org/10.1021/jp3062866.
[47] T. Björkman, V. Skakalova, S. Kurasch, U. Kaiser, J.C. Meyer, J.H. Smet, et al, Vibrational properties of a two-dimensional silica Kagome Lattice, ACS Nano (2016), https://doi.org/10.1021/acsnano.6b05577.
[48] L. Lichtenstein, M. Heyde, S. Ulrich, N. Nilius, H.-J. Freund, Probing the properties of metal–oxide interfaces: silica films on Mo and Ru supports, J. Phys.: Condens. Matter 24 (2012) 354010, https://doi.org/10.1088/0953-8984/24/35/354010.
[49] C.S.S.R. Kumar, (Ed.), Surface Science Tools for Nanomaterials Characterization, Springer Berlin Heidelberg, Berlin, Heidelberg, 2015. doi:10.1007/978-3-662-44551-8.
[50] C. Büchner, L. Lichtenstein, S. Stuckenholz, M. Heyde, F. Ringleb, M. Sterrer, et al, Adsorption of Au and Pd on Ruthenium-Supported Bilayer Silica, J. Phys. Chem. C 118 (2014) 20959–20969. http://pubs.acs.org/doi/abs/10.1021/jp5055342.
[51] M. Wang, J.-Q. Zhong, J. Kestell, I. Waluyo, D.J. Stacchiola, J.A. Boscoboinik, et al, Energy Level Shifts at the Silica/Ru(0001) Heterojunction Driven by Surface and Interface Dipoles, Top. Catal. (2016), https://doi.org/10.1007/s11244-016-0704-x.
[52] P. Schlexer, L. Giordano, G. Pacchioni, Adsorption of Li, Na, K, and Mg atoms on amorphous and crystalline silica bilayers on Ru(0001): a DFT Study, J. Phys. Chem. C 118 (2014) 15884–15897.
[53] W. Raberg, K. Wandelt, Atomically resolved AFM investigations of an amorphous barium silicate surface, Appl. Phys. A Mat. Sci. Process. 66 (1998) 1143–1146.
[54] W. Raberg, A.H. Ostadrahimi, T. Kayser, K. Wandelt, Atomic scale imaging of amorphous silicate glass surfaces by scanning force microscopy, J. Non. Cryst. Solids. 351 (2005) 1089–1096, https://doi.org/10.1016/j.jnoncrysol.2005.01.022.
[55] C. Büchner, P. Schlexer, L. Lichtenstein, S. Stuckenholz, M. Heyde, H.-J. Freund, Topological Investigation of Two-Dimensional Amorphous Materials, Zeitschrift Für Phys. Chemie. 228 (2014) 587–607, https://doi.org/10.1515/zpch-2014-0438.
[56] M. Pivetta, M.-C. Blüm, F. Patthey, W.-D. Schneider, Two-Dimensional Tiling by Rubrene Molecules Self-Assembled in Supramolecular Pentagons, Hexagons, and Heptagons on a Au(111) Surface, Angew. Chemie Int. Ed. 47 (2008) 1076–1079, https://doi.org/10.1002/anie.200704479.
[57] D. Weaire, N. Rivier, Soap, cells and statistics—random patterns in two dimensions, Contemp. Phys. 25 (1984) 59–99, https://doi.org/10.1080/00107518408210979.
[58] T. Björkman, S. Kurasch, O. Lehtinen, J. Kotakoski, O.V. Yazyev, A. Srivastava, et al, Defects in bilayer silica and graphene: common trends in diverse hexagonal two-dimensional systems, Sci. Rep. 3 (2013) 3482, https://doi.org/10.1038/srep03482.
[59] P.Y. Huang, S. Kurasch, J.S. Alden, A. Shekhawat, A.A. Alemi, P.L. McEuen, et al, Imaging atomic rearrangements in two-dimensional silica glass: watching Silica's Dance, Science 80 (342) (2013) 224–227, https://doi.org/10.1126/science.1242248.
[60] K.M. Burson, C. Büchner, M. Heyde, H.-J. Freund, Assessing the amorphousness and periodicity of common domain boundaries in silica bilayers on Ru (0 0 0 1), J. Phys.: Condens. Matter 29 (2017) 35002, https://doi.org/10.1088/0953-8984/29/3/035002.
[61] W. Rosenhain, D. Ewen, The Intercrystalline Cohesion of Metals, Inst. Met. 10 (1913) 119–149.
[62] D. Akinwande, C.J. Brennan, J.S. Bunch, P. Egberts, J.R. Felts, H. Gao, et al, A review on mechanics and mechanical properties of 2D materials – graphene and beyond, Extrem. Mech. Lett. 13 (2016) 1–86, https://doi.org/10.1016/j.eml.2017.01.008.
[63] B. Yang, E. Emmez, W.E. Kaden, X. Yu, J.A. Boscoboinik, M. Sterrer, et al, Hydroxylation of Metal-Supported Sheet-Like Silica Films, J. Phys. Chem.C. 117 (2013) 8336–8344, https://doi.org/10.1021/jp401935u.
[64] A.C. Wright, M.F. Thorpe, Eighty years of random networks, Phys. Status Solidi Basic Res. 250 (2013) 931–936, https://doi.org/10.1002/pssb.201248500.
[65] S.K. Sharma, J.F. Mammone, M.F. Nicol, Raman investigation of ring configurations in viterous silica, Nature 292 (1981) 140–141, https://doi.org/10.1038/292140a0.
[66] J.F. Shackelford, J.S. Masaryk, The interstitial structure of vitreous silica, J. Non. Cryst. Solids. 30 (1978) 127–134, https://doi.org/10.1016/0022-3093(78)90061-3.
[67] W.H. Zachariasen, The Atomic Arrangement in Glass, J. Am. Chem. Soc. 54 (1932) 3841–3851, https://doi.org/10.1021/ja01349a006.
[68] J.F. Shackelford, Triangle rafts — extended Zachariasen schematics for structure modeling, J. Non. Cryst. Solids. 49 (1982) 19–28, https://doi.org/10.1016/0022-3093(82)90106-5.
[69] C. Büchner, L. Liu, S. Stuckenholz, K.M. Burson, L. Lichtenstein, M. Heyde, et al, Building block analysis of 2D amorphous networks reveals medium range correlation, J. Non. Cryst. Solids. 435 (2016) 40–47, https://doi.org/10.1016/j.jnoncrysol.2015.12.020.
[70] J.F. Shackelford, B.D.D. Brown, The lognormal distribution in the random network structure, J. Non. Cryst. Solids. 44 (1981) 379–382, https://doi.org/10.1016/0022-3093(81)90040-5.
[71] A. Kumar, D. Sherrington, M. Wilson, M.F. Thorpe, Ring statistics of silica bilayers, J. Phys.: Condens. Matter 26 (2014) 395401, https://doi.org/10.1088/0953-8984/26/39/395401.
[72] S.N. Chiu, Aboav-Weaire's and Lewis' Laws – a review, Mater. Charact. 34 (1995) 149–165, https://doi.org/10.1016/1044-5803(94)00081-U.
[73] F.T. Lewis, A comparison between the mosaic of polygons in a film of artificial emulsion and the pattern of simple ephithelium in surface view (cucumber epidermis and human amnion), Anat. Rec. 50 (1931) 235–265, https://doi.org/10.1002/ar.1090500303.
[74] M. Sadjadi, M.F. Thorpe, Ring correlations in random networks, Phys. Rev. E. 94 (2016) 62304, https://doi.org/10.1103/PhysRevE.94.062304.
[75] C. Büchner, L. Lichtenstein, M. Heyde, H.-J. Freund, The atomic structure of two-dimensional silica, in: Noncontact At. Force Microsc., vol. 3, 2015: pp. 327–353. doi:10.1007/978-3-319-15588-3_16.
[76] K. Takayanagi, Y. Tanishiro, M. Takahashi, S. Takahashi, Structural analysis of Si(111)-7×7 by UHV-transmission electron diffraction and microscopy, J. Vac. Sci. Technol. A Vacuum, Surfaces, Film 3 (1985) 1502, https://doi.org/10.1116/1.573160.
[77] Y. Li, D.A. Drabold, Symmetry breaking and low energy conformational fluctuations in amorphous graphene, Phys. Status Solidi B Basic Solid State Phys. 250 (2013) 1012–1019, https://doi.org/10.1002/pssb.201248481.
[78] F. Yang, Y. Choi, P. Liu, D. Stacchiola, J. Hrbek, J.A. Rodriguez, Identification of 5–7 defects in a copper oxide surface, J. Am. Chem. Soc. 133 (2011) 11474–11477, https://doi.org/10.1021/ja204652v.
[79] M.O. Blunt, J.C. Russell, N.R. Champness, P.H. Beton, Templating molecular adsorption using a covalent organic framework, Chem. Commun. (Cambridge, United Kingdom) 46 (2010) 7157–7159, https://doi.org/10.1039/c0cc01810d.
[80] J.A. Boscoboinik, X. Yu, B. Yang, S.K. Shaikhutdinov, H.-J. Freund, Building blocks of zeolites on an aluminosilicate ultra-thin film, Microporous Mesoporous Mater. 165 (2013) 158–162, https://doi.org/10.1016/j.micromeso.2012.08.014.
[81] S. Maier, B.A.J. Lechner, G.A. Somorjai, M. Salmeron, Growth and Structure of the First Layers of Ice on Ru(0001) and Pt(111), J. Am. Chem. Soc. 138 (2016) 3145–3151, https://doi.org/10.1021/jacs.5b13133.
[82] D. Shechtman, I. Blech, D. Gratias, J.W. Cahn, Metallic Phase with Long-Range Orientational Order and No Translational Symmetry, Phys. Rev. Lett. 53 (1984) 1951–1953, https://doi.org/10.1103/PhysRevLett. 53.1951.

Please cite this article in press as: C. Büchner, M. Heyde, Two-dimensional silica opens new perspectives, Prog. Surf. Sci (2017), https://doi.org/10.1016/j.progsurf.2017.09.001

[83] B. Hargittai, Science of Crystal Structures, Springer International Publishing, Cham (2015), https://doi.org/10.1007/978-3-319-19827-9.
[84] S. Förster, K. Meinel, R. Hammer, M. Trautmann, W. Widdra, Quasicrystalline structure formation in a classical crystalline thin-film system, Nature 502 (2013) 215–218, https://doi.org/10.1038/nature12514.
[85] J.I. Urgel, D. Écija, G. Lyu, R. Zhang, C.-A. Palma, W. Auwärter, et al, Quasicrystallinity expressed in two-dimensional coordination networks, Nat. Chem. 8 (2016) 657–662, https://doi.org/10.1038/nchem.2507.
[86] K.M. Burson, P. Schlexer, C. Büchner, L. Lichtenstein, M. Heyde, H.-J. Freund, Characterizing crystalline-vitreous structures: from atomically resolved silica to macroscopic bubble rafts, J. Chem. Educ. 92 (2015) 1896–1902, https://doi.org/10.1021/acs.jchemed.5b00056.
[87] S. Stuckenholz, C. Büchner, M. Heyde, H.-J. Freund, MgO on Mo(001): local work function measurements above pristine terrace and line defect sites, J. Phys. Chem. C 119 (2015) 12283–12290, https://doi.org/10.1021/jp512575n.
[88] R.P. Feynman, There's plenty of room at the bottom, Eng. Sci. 23 (1960) 22–36.
[89] Y. Wang, Z. Song, Z. Xu, Mechanistic transition of heat conduction in two-dimensional solids: a study of silica bilayers, Phys. Rev. B. 92 (2015) 245427, https://doi.org/10.1103/PhysRevB.92.245427.
[90] Z. Xu, Heat transport in low-dimensional materials: a review and perspective, Theor. Appl. Mech. Lett. 6 (2016) 113–121, https://doi.org/10.1016/j.taml.2016.04.002.
[91] E. Abrahams, P.W. Anderson, D.C. Licciardello, T.V. Ramakrishnan, Scaling Theory of localization: absence of quantum diffusion in two dimensions, Phys. Rev. Lett. 42 (1979) 673–676, https://doi.org/10.1103/PhysRevLett. 42.673.
[92] J. Zhang, Phase transformation in two-dimensional crystalline silica under compressive loading, Phys. Chem. Chem. Phys. 19 (2017) 8478–8484, https://doi.org/10.1039/C7CP00273D.
[93] R. Wiesendanger, M. Ringger, L. Rosenthaler, H.R. Hidber, P. Oelhafen, H. Rudin, et al, Application of Scanning Tunneling Microscopy to Disordered Systems, Surf. Sci. 181 (1987) 46–54, https://doi.org/10.1016/0039-6028(87)90140-3.
[94] D.E. Bürgler, C.M. Schmidt, D.M. Schaller, F. Meisinger, T.M. Schaub, A. Baratoff, et al, Atomic-scale scanning tunneling microscopy of amorphous surfaces, Phys. Rev. B Condens. Matter Mater. Phys. 59 (1999) 895–902, https://doi.org/10.1103/PhysRevB.59.10895.
[95] J.-F. Poggemann, A. Goß, G. Heide, E. Rädlein, G.H. Frischat, Direct view of the structure of a silica glass fracture surface, J. Non. Cryst. Solids. 281 (2001) 221–226.
[96] C. Büchner, L. Lichtenstein, M. Heyde, Ein glasklares Modell, Nachrichten Aus Der Chemie. 60 (2012) 861–864.
[97] T.M. Schaub, D.E. Bürgler, C.M. Schmidt, H. Güntherodt, Investigation of non-crystalline surfaces by scanning tunneling microscopy, J. Non. Cryst. Solids. 205–207 (1996) 748–754.
[98] G. Kumar, P.A. Staffier, J. Blawzdziewicz, U.D. Schwarz, J. Schroers, Atomically smooth surfaces through thermoplastic forming of metallic glass, Appl. Phys. Lett. 97 (2010) 101907, https://doi.org/10.1063/1.3485298.
[99] S. Morita, R. Wiesendanger, E. Meyer, (Eds.), Noncontact Atomic Force Microscopy, Springer Berlin Heidelberg, Berlin, Heidelberg, 2002. doi:10.1007/978-3-642-56019-4.
[100] M. Heyde, G.H. Simon, H.-P. Rust, H.-J. Freund, Probing adsorption sites on thin oxide films by dynamic force microscopy, Appl. Phys. Lett. 89 (2006) 263107, https://doi.org/10.1063/1.2424432.
[101] L. Lichtenstein, C. Büchner, S. Stuckenholz, M. Heyde, H.-J. Freund, Enhanced atomic corrugation in dynamic force microscopy—The role of repulsive forces, Appl. Phys. Lett. 100 (2012) 123105, https://doi.org/10.1063/1.3696039.
[102] K.M. Burson, L. Gura, B. Kell, C. Büchner, A.L. Lewandowski, M. Heyde, et al, Resolving amorphous solid-liquid interfaces by atomic force microscopy, Appl. Phys. Lett. 108 (2016) 201602, https://doi.org/10.1063/1.4949556.
[103] J.A. Boscoboinik, X. Yu, B. Yang, F.D. Fischer, R. Włodarczyk, M. Sierka, et al, Modeling Zeolites with Metal-Supported Two-Dimensional Aluminosilicate Films, Angew. Chemie Int. Ed. 51 (2012) 6005–6008, https://doi.org/10.1002/anie.201201319.
[104] R. Włodarczyk, J. Sauer, X. Yu, J.A. Boscoboinik, B. Yang, S.K. Shaikhutdinov, et al, Atomic Structure of an Ultrathin Fe-Silicate Film Grown on a Metal: a Monolayer of Clay?, J Am. Chem. Soc. 135 (2013) 19222–19228, https://doi.org/10.1021/ja408772p.
[105] F.D. Fischer, J. Sauer, X. Yu, J.A. Boscoboinik, S.K. Shaikhutdinov, H.-J. Freund, Ultrathin Ti-Silicate Film on a Ru(0001) Surface, J. Phys. Chem. C 119 (2015) 15443–15448, https://doi.org/10.1021/acs.jpcc.5b04291.
[106] S. Ulrich, N. Nilius, H.-J. Freund, U. Martinez, L. Giordano, G. Pacchioni, Realization of an atomic sieve: silica on Mo(112), Surf. Sci. 603 (2009) 1145–1149, https://doi.org/10.1016/j.susc.2009.02.030.
[107] P.M. Price, J.H. Clark, D.J. Macquarrie, Modified silicas for clean technology, J. Chem. Soc. Dalt. Trans. (2000) 101–110, https://doi.org/10.1039/a905457j.
[108] P.K. Jal, S. Patel, B.K. Mishra, Chemical modification of silica surface by immobilization of functional groups for extractive concentration of metal ions, Talanta 62 (2004) 1005–1028, https://doi.org/10.1016/j.talanta.2003.10.028.
[109] J. Biscoe, X-ray study of soda-lime-silica glass, J. Am. Ceram. Soc. 24 (1941) 262–264, https://doi.org/10.1111/j.1151-2916.1941.tb14859.x.
[110] H.A. Schaeffer, R. Langfeld, Werkstoff Glas, first ed. 2014 Springer Berlin, Heidelberg. http://dx.doi.org/10.1007/978-3-642-37231-5.
[111] W. Loewenstein, The distribution of aluminum in the tetrahedra of silicates and aluminateS, Am. Mineral. 39 (1954) 92–96. http://www.minsocam.org/ammin/AM39/AM39_92.pdf.
[112] L. Li, H. Tissot, S.K. Shaikhutdinov, H.-J. Freund, Transition Metal Induced Crystallization of Ultrathin Silica Films, Chem. Mater. 29 (2017) 931–934, https://doi.org/10.1021/acs.chemmater.6b05213.
[113] H. Tissot, L. Li, S.K. Shaikhutdinov, H.-J. Freund, Preparation and structure of Fe-containing aluminosilicate thin films, Phys. Chem. Chem. Phys. 18 (2016) 25027–25035, https://doi.org/10.1039/C6CP03460H.
[114] S. Wendt, M. Frerichs, T. Wei, M.S. Chen, V. Kempter, D.W. Goodman, The interaction of water with silica thin films grown on Mo(112), Surf. Sci. 565 (2004) 107–120, https://doi.org/10.1016/j.susc.2004.06.213.
[115] S. Kaya, J. Weissenrieder, D. Stacchiola, S.K. Shaikhutdinov, H.-J. Freund, Formation of an Ordered Ice Layer on a Thin Silica Film, J. Phys. Chem. C 111 (2007) 759–764, https://doi.org/10.1021/jp064283e.
[116] X. Yu, E. Emmez, Q. Pan, B. Yang, S. Pomp, W.E. Kaden, et al, Electron stimulated hydroxylation of a metal supported silicate film, Phys. Chem. Chem. Phys. 18 (2016) 3755–3764, https://doi.org/10.1039/C5CP06852E.
[117] W.E. Kaden, S. Pomp, M. Sterrer, H.-J. Freund, Insights into Silica Bilayer Hydroxylation and Dissolution, Top. Catal. (2016), https://doi.org/10.1007/s11244-016-0715-7.
[118] E. Groppo, C. Lamberti, S. Bordiga, G. Spoto, a Zecchina, The structure of active centers and the ethylene polymerization mechanism on the Cr/SiO2 catalyst: a frontier for the characterization methods, Chem. Rev. 105 (2005) 115–184, https://doi.org/10.1021/cr040083s.
[119] D. Jeremic, Polyethylene, in: Ullmann's Encycl. Ind. Chem., Wiley-VCH Verlag GmbH & Co. KGaA, Weinheim, Germany, 2014: pp. 1–42. doi:10.1002/14356007.a21_487.pub3.
[120] S. Ulrich, N. Nilius, H.-J. Freund, U. Martinez, L. Giordano, G. Pacchioni, Modifying the Adsorption Characteristic of Inert Silica Films by Inserting Anchoring Sites, Phys. Rev. Lett. 102 (2009) 110–113, https://doi.org/10.1103/PhysRevLett. 102.016102.
[121] H. Scholze, Glas, Springer, Berlin Heidelberg, Berlin, Heidelberg (1988), https://doi.org/10.1007/978-3-662-07495-4.
[122] J.-Q. Zhong, J. Kestell, I. Waluyo, S. Wilkins, C. Mazzoli, A. Barbour, et al, Oxidation and reduction under cover: chemistry at the confined space between ultrathin nanoporous silicates and Ru(0001), J. Phys. Chem. C 120 (2016) 8240–8245, https://doi.org/10.1021/acs.jpcc.6b02851.
[123] E. Emmez, J. Anibal Boscoboinik, S. Tenney, P. Sutter, S.K. Shaikhutdinov, H.J. Freund, Oxidation of the Ru(0001) surface covered by weakly bound, ultrathin silicate films, Surf. Sci. 646 (2016) 19–25, https://doi.org/10.1016/j.susc.2015.06.019.
[124] E. Emmez, B. Yang, S.K. Shaikhutdinov, H.-J. Freund, Permeation of a Single-Layer SiO2 Membrane and Chemistry in Confined Space, J. Phys. Chem. C 118 (2014) 29034–29042.

Please cite this article in press as: C. Büchner, M. Heyde, Two-dimensional silica opens new perspectives, Prog. Surf. Sci (2017), https://doi.org/10.1016/j.progsurf.2017.09.001

[125] J.A. Boscoboinik, X. Yu, E. Emmez, B. Yang, S.K. Shaikhutdinov, F.D. Fischer, et al, Interaction of probe molecules with bridging hydroxyls of two-dimensional zeolites: a surface science approach, J. Phys. Chem. C 117 (2013) 13547–13556, https://doi.org/10.1021/jp405533s.
[126] M.E. McKenzie, S. Goyal, S.H. Lee, H. Park, E. Savoy, A.R. Rammohan, et al, Adhesion of organic molecules on silica surfaces: a Density Functional Theory Study, J. Phys. Chem. C 121 (2017) 392–401, https://doi.org/10.1021/acs.jpcc.6b10394.
[127] R. Poli, (Ed.), Effects of Nanoconfinement on Catalysis, Springer International Publishing, Cham, 2017. doi:10.1007/978-3-319-50207-6.
[128] L. Ferrighi, M. Datteo, G. Fazio, C. Di Valentin, Catalysis under cover: enhanced reactivity at the interface between (Doped) graphene and anatase TiO_2, J. Am. Chem. Soc. 138 (2016) 7365–7376, https://doi.org/10.1021/jacs.6b02990.
[129] P. Schlexer, G. Pacchioni, R. Włodarczyk, J. Sauer, CO adsorption on a silica bilayer supported on Ru(0001), Surf. Sci. 648 (2016) 2–9, https://doi.org/10.1016/j.susc.2015.10.027.
[130] D.A. Muller, T. Sorsch, S. Moccio, F.H. Baumann, K. Evans-Lutterodt, G. Timp, The electronic structure at the atomic scale of ultrathin gate oxides, Nature 399 (1999) 758–761, https://doi.org/10.1038/21602.
[131] D.J. Stacchiola, M. Baron, S. Kaya, J. Weissenrieder, S.K. Shaikhutdinov, H.-J. Freund, Growth of stoichiometric subnanometer silica films, Appl. Phys. Lett. 92 (2008) 11911, https://doi.org/10.1063/1.2824842.
[132] Y.J. Chabal, Fundamental Aspects of Silicon Oxidation, first ed., 2001, Springer-Verlag Berlin, Heidelberg. doi: 10.1007/978-3-642-56711-7.
[133] A.N. Rudenko, F.J. Keil, M.I. Katsnelson, A.I. Lichtenstein, Interfacial interactions between local defects in amorphous SiO2 and supported graphene, Phys. Rev. B. 84 (2011) 1–9, https://doi.org/10.1103/PhysRevB.84.085438.
[134] R. Larciprete, P. Lacovig, F. Orlando, M. Dalmiglio, L. Omiciuolo, A. Baraldi, et al, Chemical gating of epitaxial graphene through ultrathin oxide layers, Nanoscale. 7 (2015) 12650–12658, https://doi.org/10.1039/C5NR02936H.
[135] K.S. Novoselov, A.K. Geim, S.V. Morozov, D. Jiang, Y. Zhang, S.V. Dubonos, et al, Electric field effect in atomically thin carbon films, Science 80 (306) (2004) 666–669, https://doi.org/10.1126/science.1102896.
[136] S. Tongay, J. Zhou, C. Ataca, K. Lo, T.S. Matthews, J. Li, et al, Thermally Driven Crossover from Indirect toward Direct Bandgap in 2D Semiconductors: $MoSe_2$ versus MoS_2, Nano Lett. 12 (2012) 5576–5580, https://doi.org/10.1021/nl302584w.
[137] K.F. Mak, C. Lee, J. Hone, J. Shan, T.F. Heinz, Atomically thin MoS2: a new direct-gap semiconductor, Phys. Rev. Lett. 105 (2010) 136805, https://doi.org/10.1103/PhysRevLett. 105.136805.
[138] L. Liang, J. Wang, W. Lin, B.G. Sumpter, V. Meunier, M. Pan, Electronic Bandgap and Edge Reconstruction in Phosphorene Materials, Nano Lett. 14 (2014) 6400–6406, https://doi.org/10.1021/nl502892t.
[139] L. Song, L. Ci, H. Lu, P.B. Sorokin, C. Jin, J. Ni, et al, Large Scale Growth and Characterization of Atomic Hexagonal Boron Nitride Layers, Nano Lett. 10 (2010) 3209–3215, https://doi.org/10.1021/nl1022139.

Please cite this article in press as: C. Büchner, M. Heyde, Two-dimensional silica opens new perspectives, Prog. Surf. Sci (2017), https://doi.org/10.1016/j.progsurf.2017.09.001